On the existence of subtropical anticyclone with equivalent-barotropic structure over Japan in August.

ENOMOTO Takeshi, *
MATSUDA Yoshihisa†, Brian J. Hoskins‡

5 December 2000

Abstract

The equivalent-barotropic structure of Bonin high is examined with a simple GCM and re-analysis data. The stationary Rossby wave induced in the desert region is found to be responsible for the equivalent-barotropic structure near Japan. The present talk begins with a classical problem on the response to heating. Realistic settings such as effects of zonal flow and orography are gradually added.

*Corresponding author, The University of Tokyo
†The University of Tokyo
‡The University of Reading

FDEPS 2000

Plan of talk

1. Introduction

2. Response to localised heating

   - Response to heating on the equator
   - Response to off-equatorial heating
   - Role of zonal flow
   - Effect of orography

3. Response to climatological heating

   - Total climatological heating of August
   - Total but the Western Pacific heating
   - Total but the Silk Road cooling

4. Conclusions and Discussion

Equivalent-barotropic structure of Bonin high

- Develops and covers Japan after the Baiu season.
- Equivalent-barotropic:
  - Vertically in phase
  - Maximum amplitude near the tropopause
- Quasi-stationary: $\sim$ 10-15 days

Charts: 31 July 2000

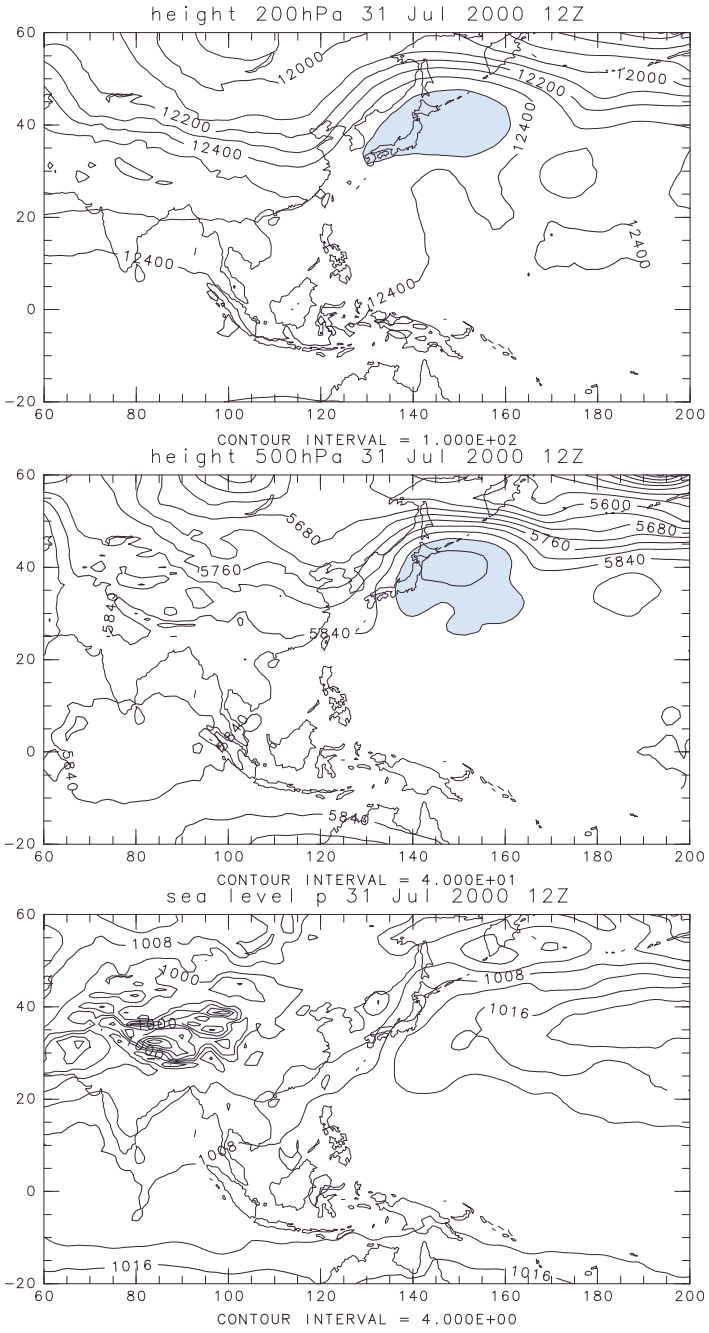

Figure 1: 200, 500 hPa height and sea level pressure

Observed diabatic heating

- Major heatings:
  - Bay of Bengal – Indian monsoon, off-equatorial
  - Western Pacific – Asian monsoon
- Cooling: Silk Road

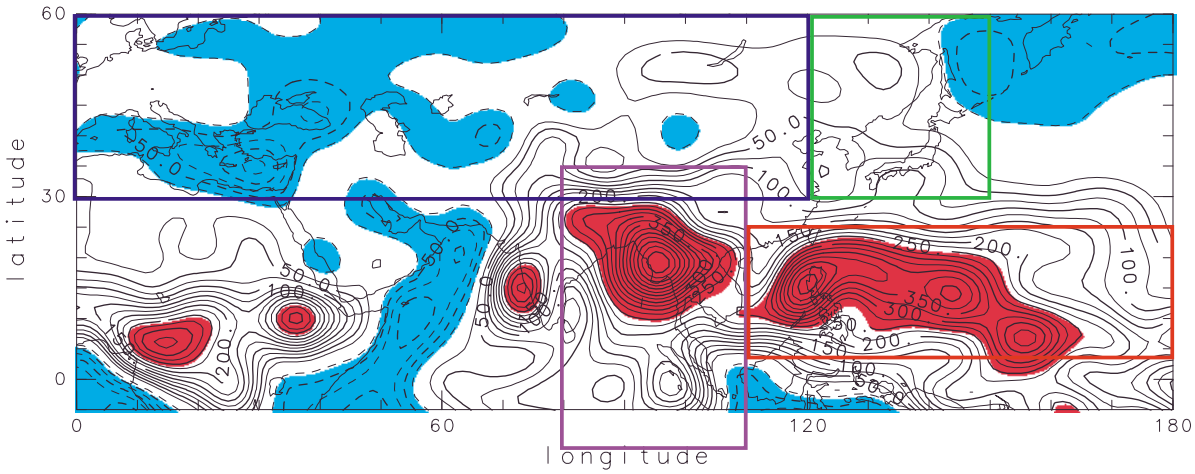

Figure 2: Column integrated diabatic heating in August (ERA15 climatology) in $\mathrm{W/m^2}$

8月の気候値に見る小笠原高気圧の等価順圧構造

流線函数（東西平均からのずれ）

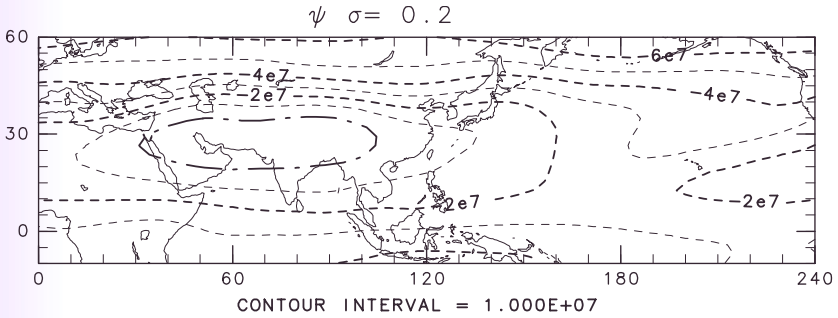

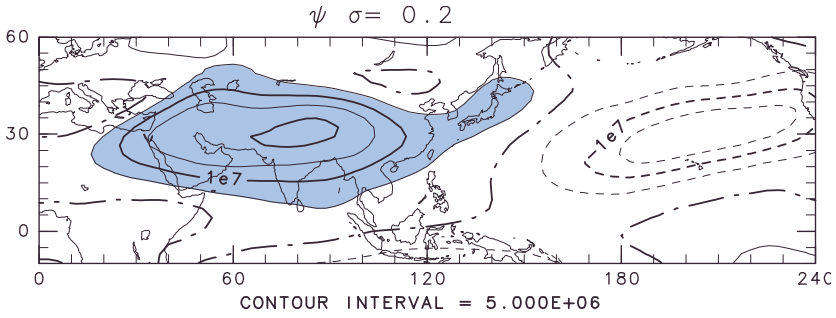

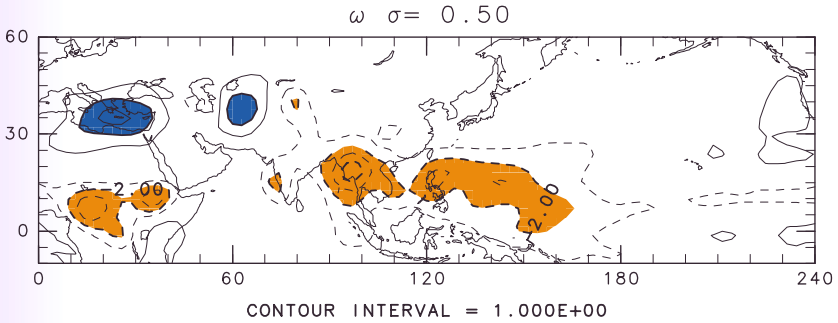

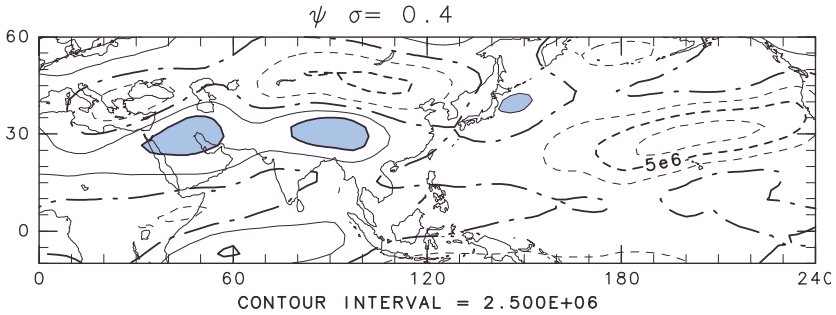

流線函数（東西平均からのずれ）

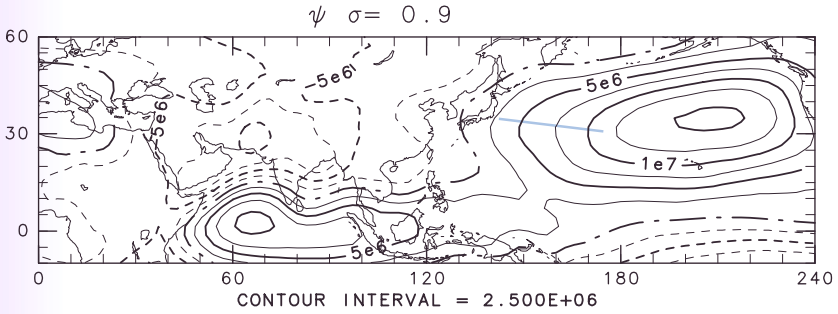

Response to heating on the equator

Matsuno (1966)'s model:

- Shallow water
- Equatorial β plane
- Linearised about the stationary atmosphere

Assuming $L_x \gg L_y$, the set equations become:

$$\frac{\partial u}{\partial t} - \beta y v = -\frac{\partial \phi}{\partial x} \tag{1}$$

$$\beta y u = -\frac{\partial \phi}{\partial y} \tag{2}$$

$$\frac{\partial \phi}{\partial t} + gh\left(\frac{\partial u}{\partial x} + \frac{\partial v}{\partial y}\right) = 0. \tag{3}$$

Kelvin wave

If $v = 0$, Eqs. (1)-(3) become

$$\frac{\partial u}{\partial t} = -\frac{\partial \phi}{\partial x} \tag{4}$$

$$\beta y u = -\frac{\partial \phi}{\partial y} \tag{5}$$

$$\frac{\partial \phi}{\partial t} + gh\left(\frac{\partial u}{\partial x}\right) = 0. \tag{6}$$

Equations (4) and (6) give

$$\frac{\partial^2 u}{\partial t^2} - gh\left(\frac{\partial^2 u}{\partial x^2}\right) = 0. \tag{7}$$

Thus the dispersion relation for the Kelvin wave is

$$c^2 = \frac{\omega^2}{k^2} = gh, \tag{8}$$

if the monochromatic wave solution

$$\begin{pmatrix} u \\ v \\ \phi \end{pmatrix} = \begin{pmatrix} \hat{u} \\ \hat{v} \\ \hat{\phi} \end{pmatrix} \exp\{i(kx - \omega t)\} \tag{9}$$

is assumed, the solution is given by Eq. (4) and (5)

$$\hat{u} = u_0 \exp\left(-\frac{y^2}{2L_\beta^2}\right), \tag{10}$$

where $L_\beta \equiv \sqrt{\sqrt{gh}/\beta}$ is the *equatorial Rossby radius of deformation*.

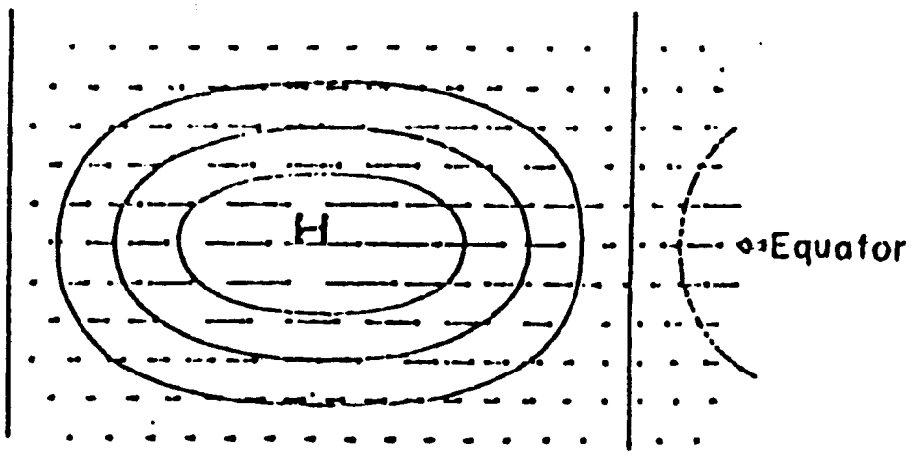

Figure 3: (u, v) and ϕ for the Kelvin wave solution

Rossby wave

For $v \neq 0$, we obtain

$$\frac{\mathrm{d}^2\hat{v}}{\mathrm{d}y^2} + \left(-\frac{\beta k}{\omega} - \frac{\beta^2 y^2}{gh}\right)\hat{v} = 0 \qquad (11)$$

from eq. (1)-(3), and (9). Substituting $Y = y/L_\beta$ and $\hat{v} = f(Y)\exp(-Y^2/2)$ into (11), we have

$$\frac{\mathrm{d}^2 f}{\mathrm{d}Y^2} - 2Y\frac{\mathrm{d}f}{\mathrm{d}Y} + \left\{-\frac{k\sqrt{gh}}{\omega} - 1\right\} f = 0 \qquad (12)$$

Equation (12) has a solution

$$f(Y) = H_n(Y) \qquad (13)$$

provided that

$$-\frac{k\sqrt{gh}}{\omega} = 2n + 1, \ (n \neq 0). \qquad (14)$$

The phase speed of the Rossby wave is

$$c = -\frac{\sqrt{gh}}{(2n+1)}, \tag{15}$$

which is slower than the phase speed of Kelvin wave at least by a factor of 3 ($n = 1$).

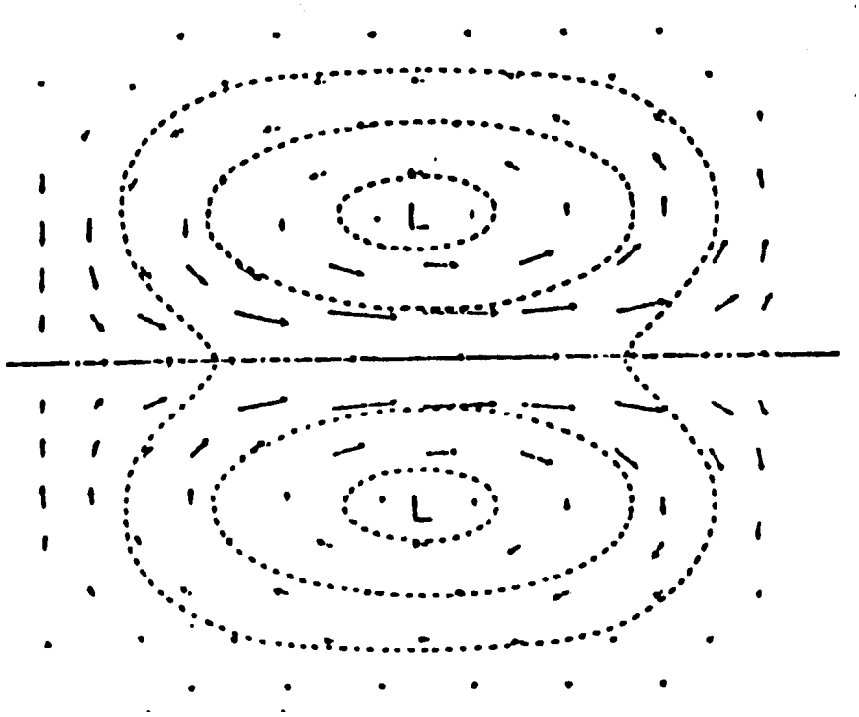

Figure 4: (u, v) and ϕ for the Rossby wave solution

Gill pattern

Solutions for heating on the equator:

- Decay away from the equator as $\exp(-y^2/4)$.
- Eastward propagating Kelvin wave
- Westward proagating Rossby wave

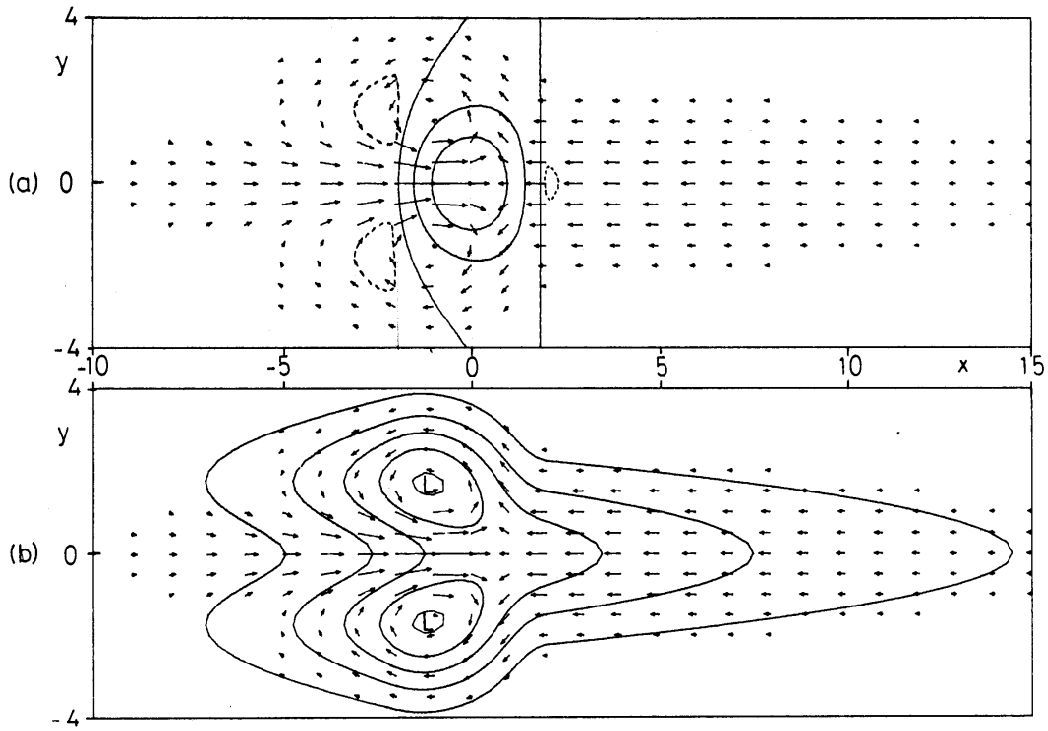

Figure 5: Distribution of (a)$(u, v), w$, (b)$(u, v), p$.

Sverdrup balance

In the heating region,

- ascent, $w > 0$, has the same pattern as Q.
- the flow is away from the heat source, $v > 0$.

The vorticity equation,

$$\beta v = -f \left(\frac{\partial u}{\partial x} + \frac{\partial v}{\partial y} \right),$$

(the Sverdrup balance) requires the poleward flow.

Response to antisymmetric heating

- Long mixed wave in the heating region.
- No motion to the east of heating.
- Westward propagating Rossby wave

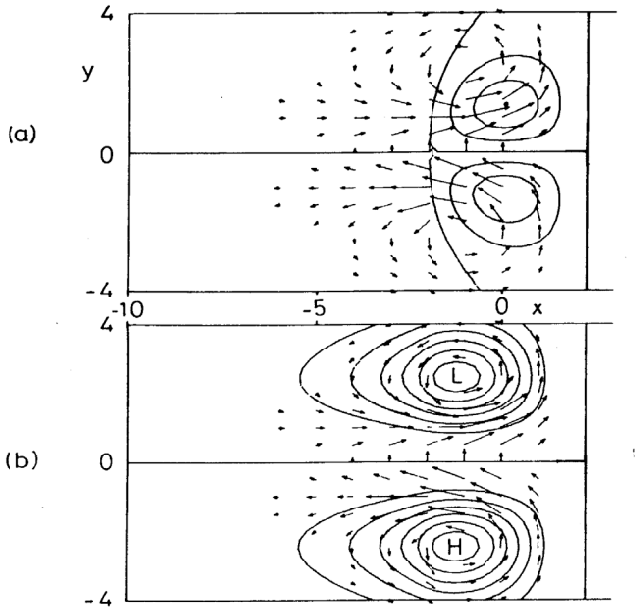

Figure 6: Distribution of (a)$(u, v), w$, (b)$(u, v), p$.

Response to off-equatorial heating

- Symmetric + antisymmetric (Gill, 1980)
- Dominatly Rossby wave to the west
- Warm region to the west
- Descent to the west (Rodwell and Hoskins, 1996)

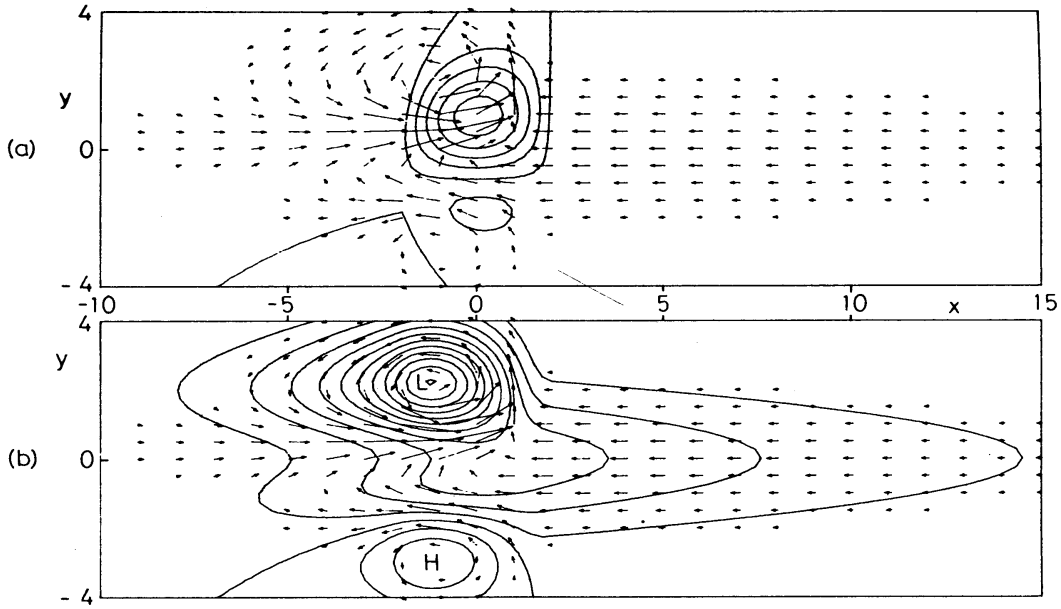

Figure 7: Distribution of (a)$(u, v), w$, (b)$(u, v), p$.

Why Sahara is dry in the summer?

- No Hadley cell in NH summer.
- But strong descent over the desert region.
- Zonal(West-East) temperature gradient due to off-equatorial heating.

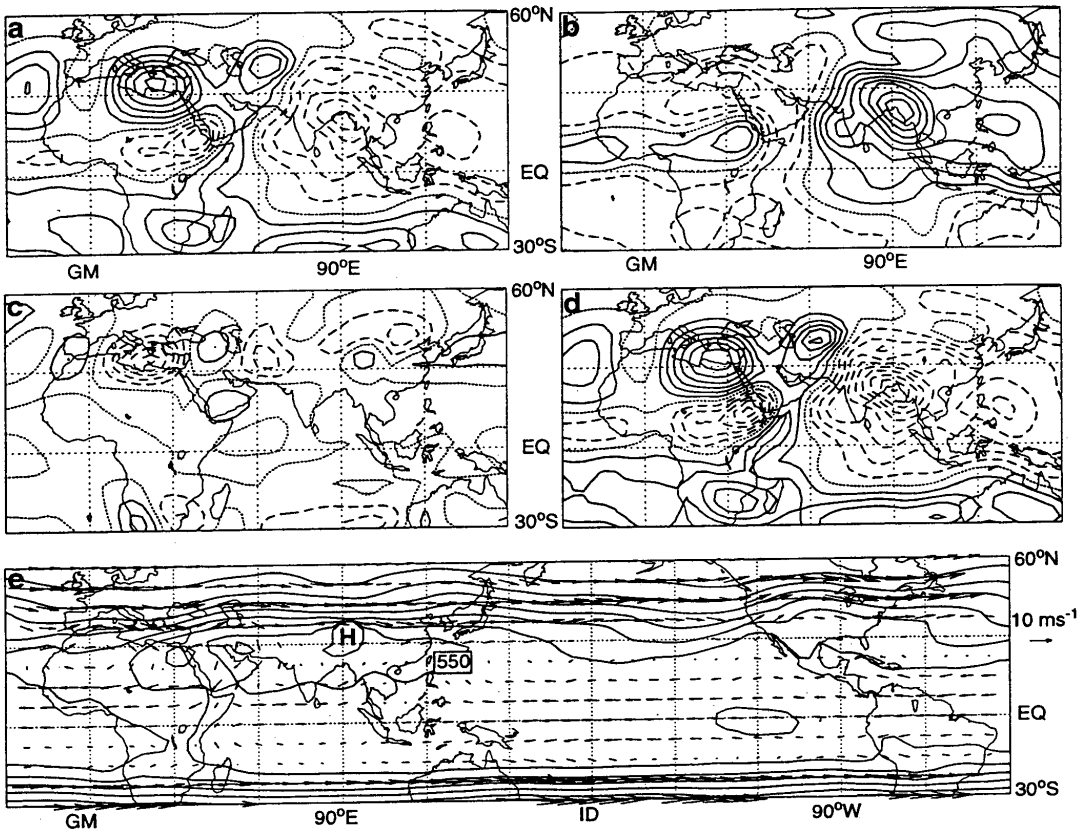

Figure 8: Observed JJA (a)ω, (b)-(d) each term of thermodynamic equation, and $(u, v), p$ on $\theta = 325\mathrm{K}$ (Rodwell and Hoskins, 1996).

Monsoon-Desert mechanism

- Monsoon heating creates a warm anomaly to the west.
- The isentropic surface lowers.
- The westerly descends along the isentropics surface.

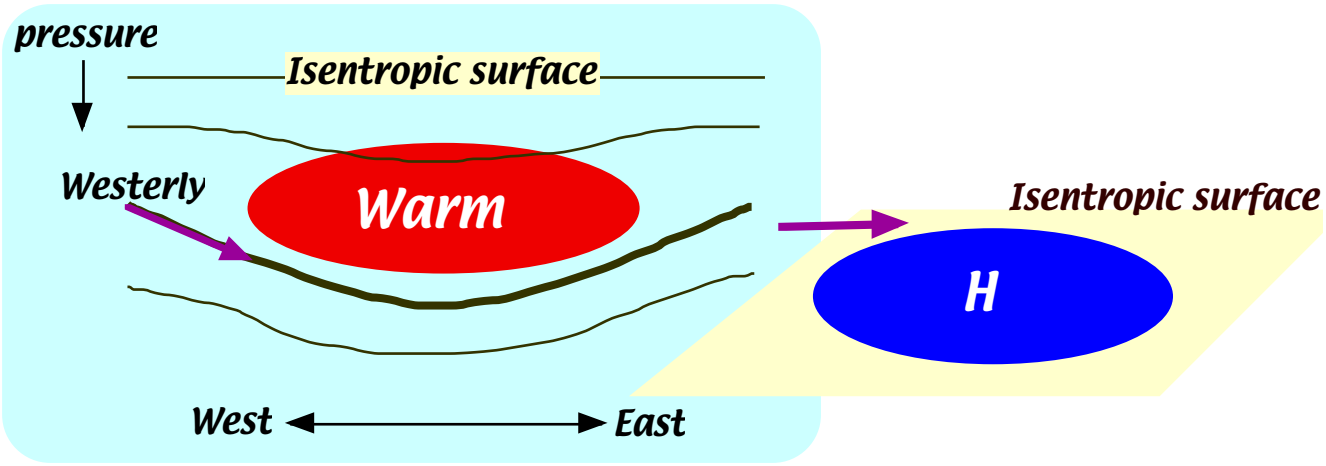

Figure 9: Schematic illustration of the Monsoon-Desert mechanism

Model and Data

Reading Univ. spectral model:

- Horizontal truncation wavenumber: 42
- Num of vertical layers: 15
- No physical processes

Climatology of August from the ECMWF re-analysis (1979-93):

- Zonally-averaged winds and temperature, or
- Globally-averaged temperature in each layer
- Diabatic heating

Experiments on response to localised heating

- Indian heating (80E–110E, 10S–35N)
- Effect of off-equatorial heating:
  Heating at the equator and at 20N
- Role of the jet
  - How does off-equatorial heating interact with the jet?
  - Re-examination of the Monsoon-Desert mechanism
- Effect of orography

Response to the Indian heating relocated to the equator

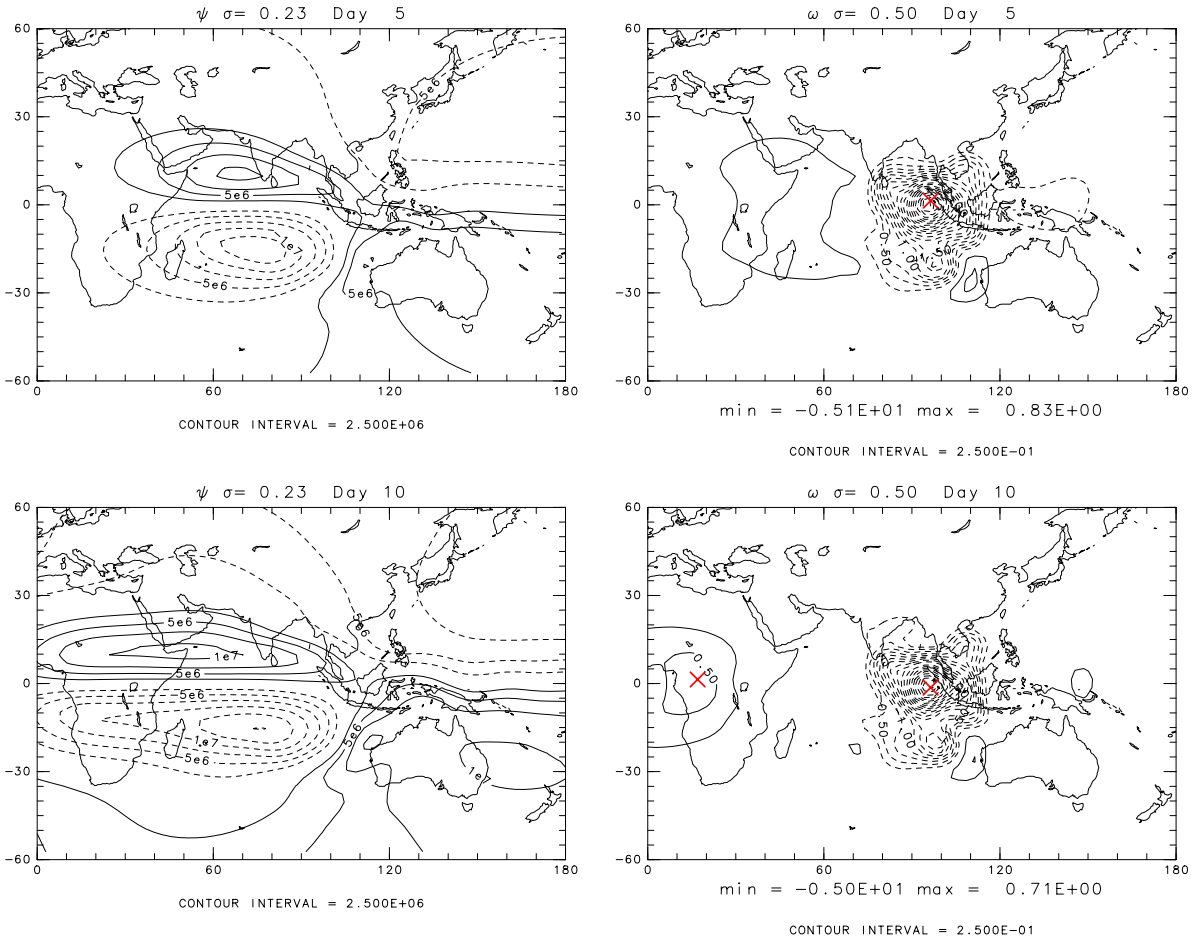

Figure 10: ψ and ω at Day 5 (top) and 10 (bottom)

Response to the Indian heating

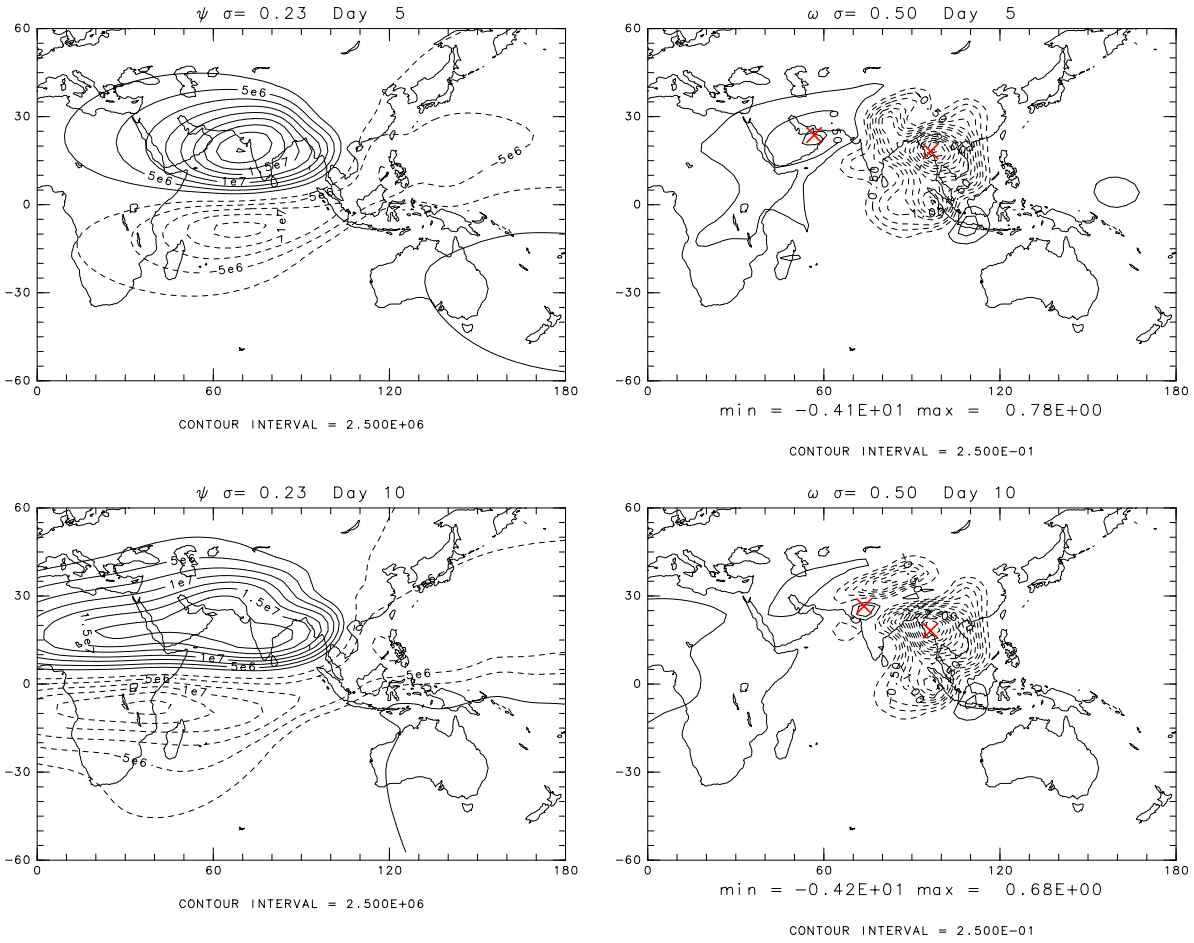

Figure 11: ψ and ω at Day 5 (top) and 10 (bottom)

Response to the Indian heating in the presence of the jet

- Descent and ascent along the jet
- Northeastward propagation of stationary Rossby Wave

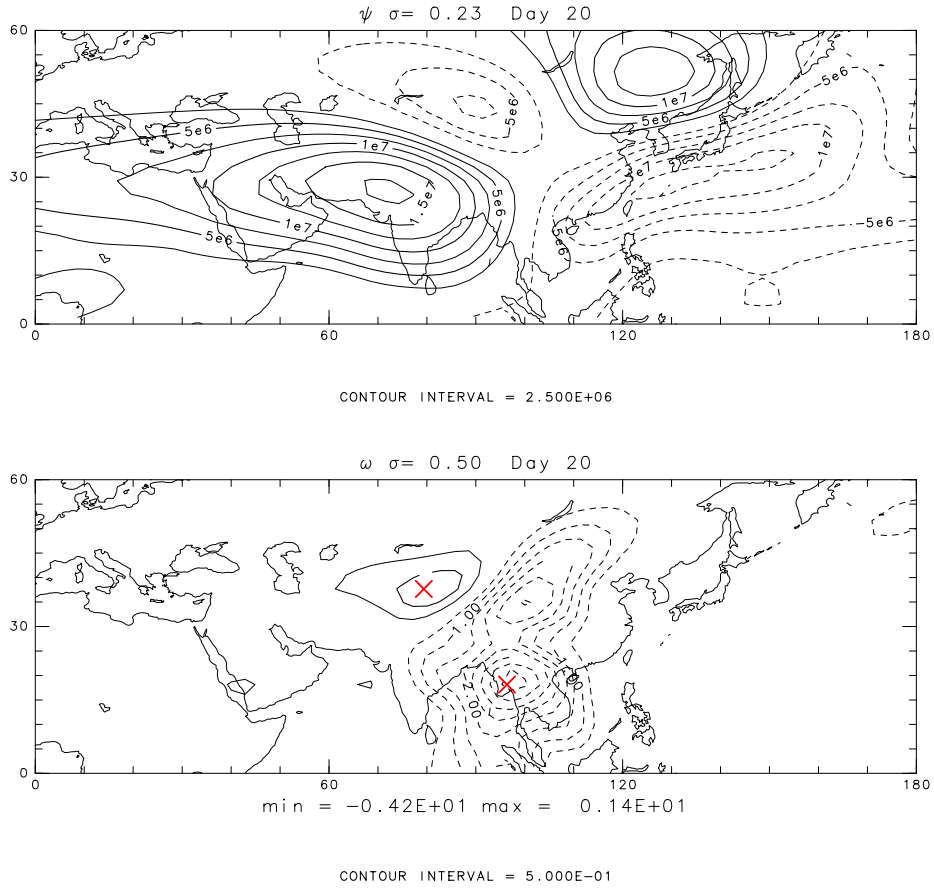

Figure 12: ψ at $\sigma = 0.23$ and ω at $\sigma = 0.5$

Descent along the isentropes

$$\frac{\partial \bar{u}}{\partial z} = -\frac{R}{H}\frac{\partial \bar{T}}{\partial y}$$

The jet is associated with the isentropes descending toward the equator.

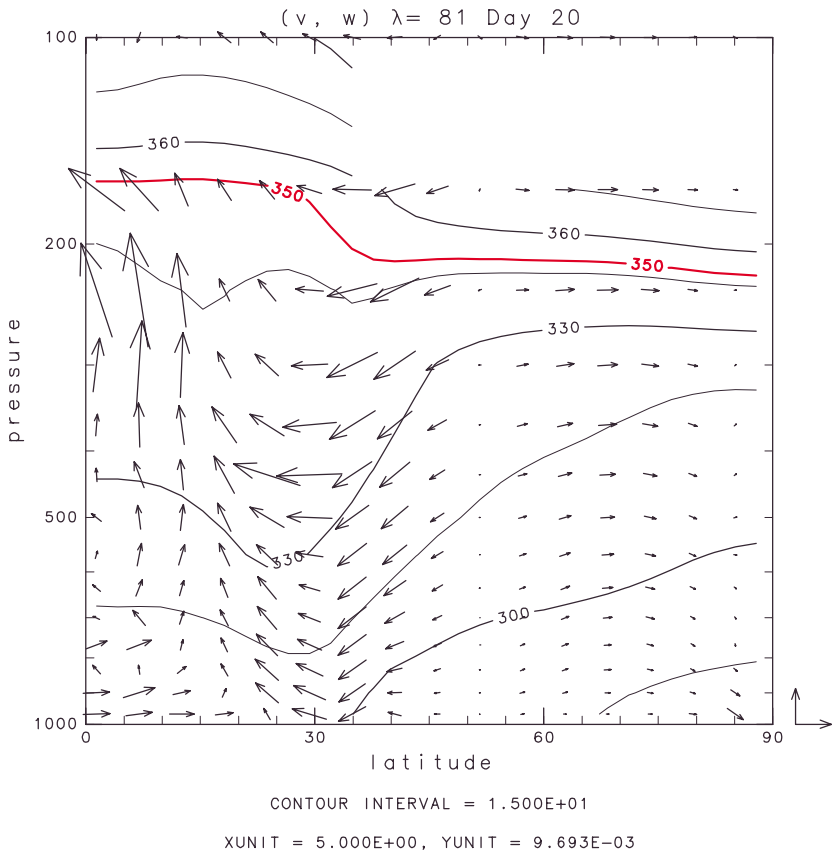

Figure 13: ϕ–p section of (v, ω), θ at $\lambda = 81$E

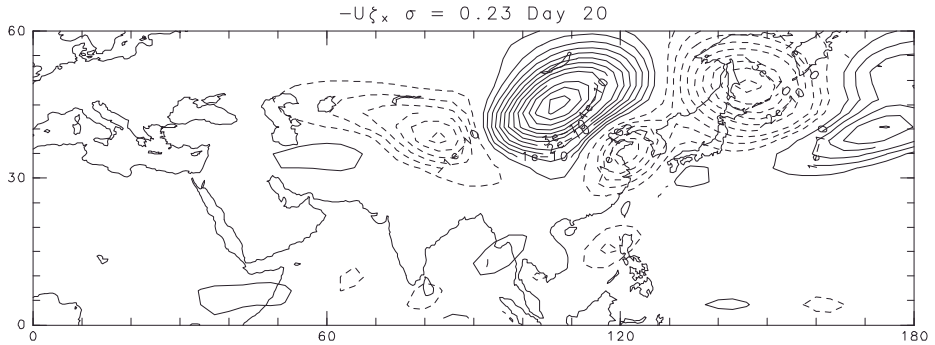

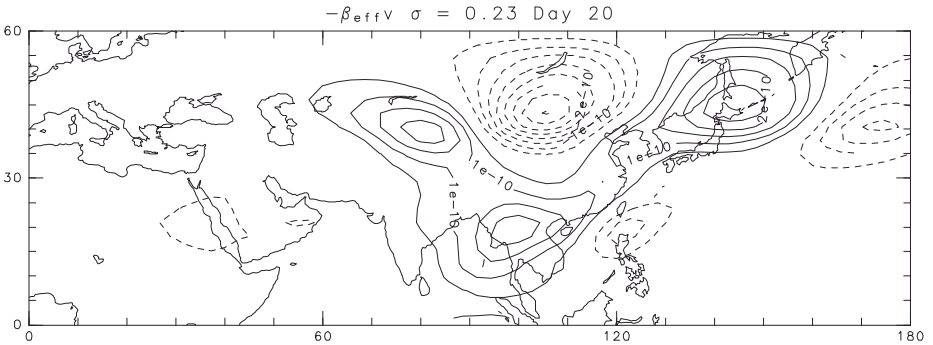

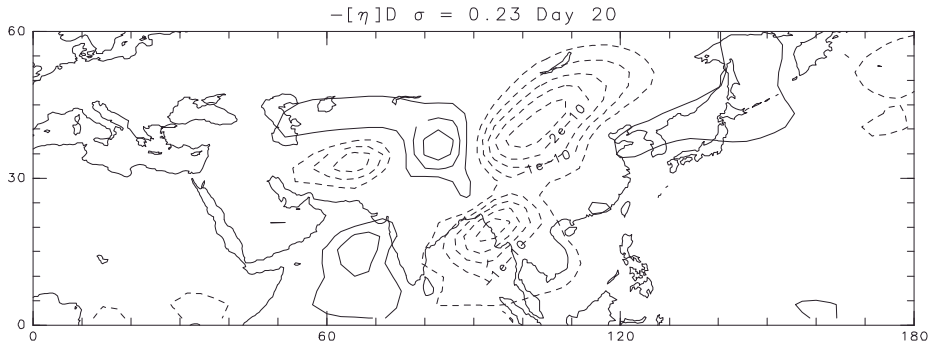

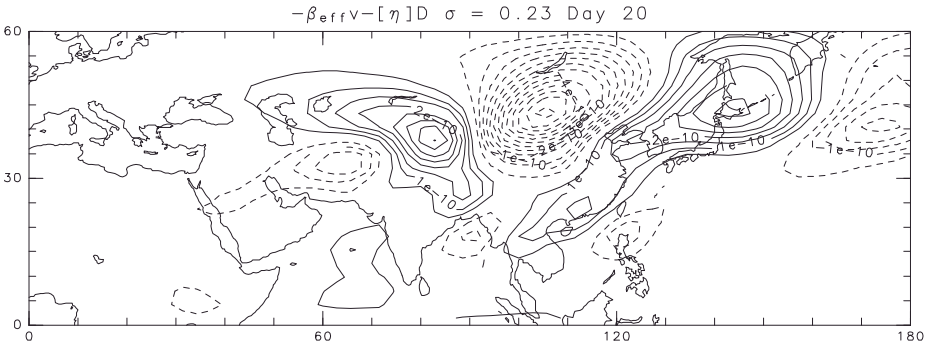

CONTOUR INTERVAL = 5.000E-11

CONTOUR INTERVAL = 5.000E-11

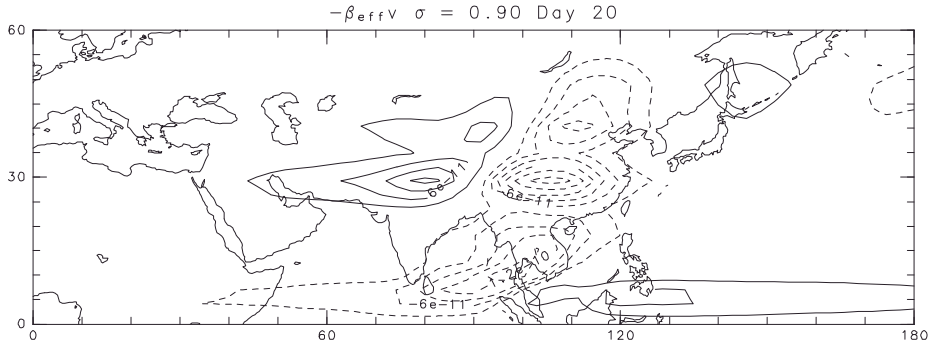

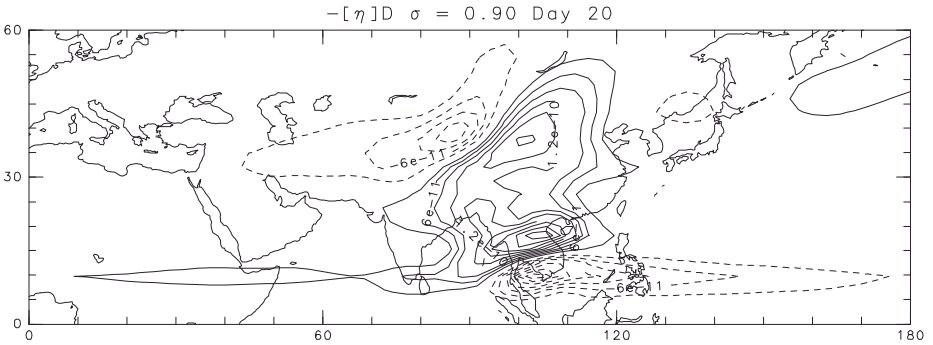

CONTOUR INTERVAL = 3.000E-11

CONTOUR INTERVAL = 3.000E-11

Vorticity balance

$$\bar{u}\frac{\partial \zeta'}{\partial x} + \beta v' = -(f+\zeta)D'$$

- In the upper troposphere, the zonal advection is balanced by the planetary vorticity advection and the stretching of vortex tube.

- In the lower troposphere, the shrinking of vortex tube is balanced by the planetary vorticity advection.

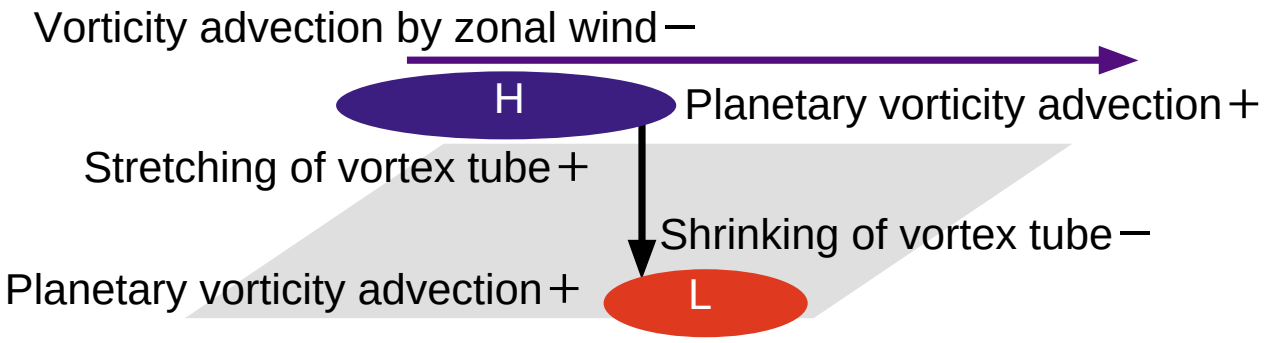

Figure 14: Schematic illustration of vorticity balance

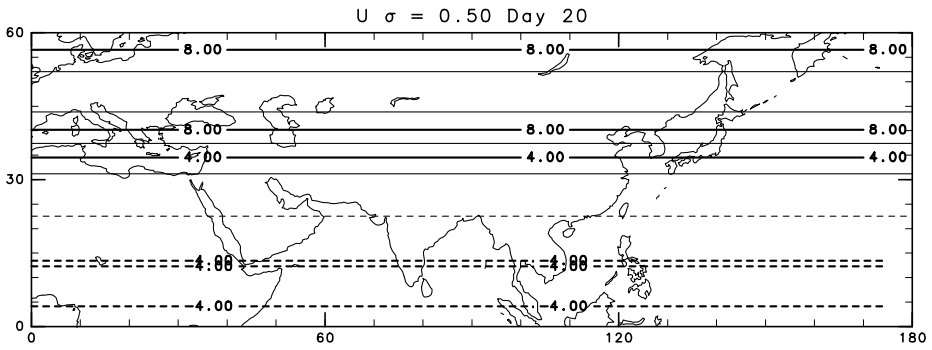

CONTOUR INTERVAL = 2.000E+00

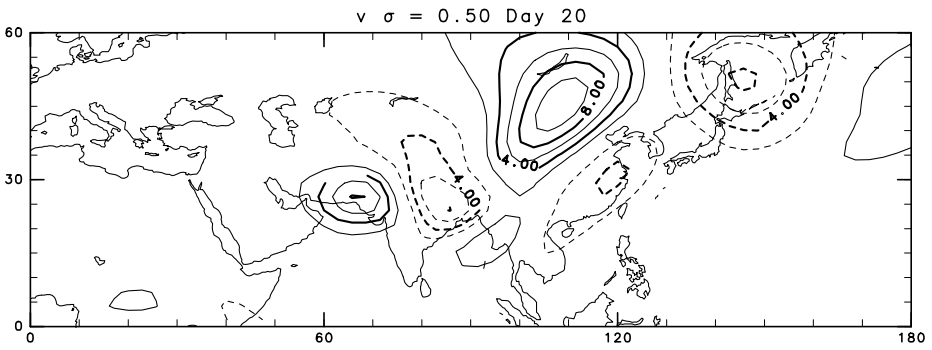

CONTOUR INTERVAL = 2.000E+00

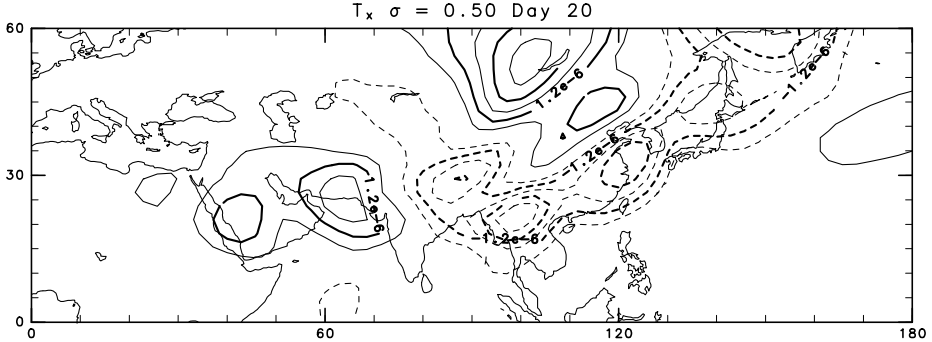

CONTOUR INTERVAL = 6.000E-07

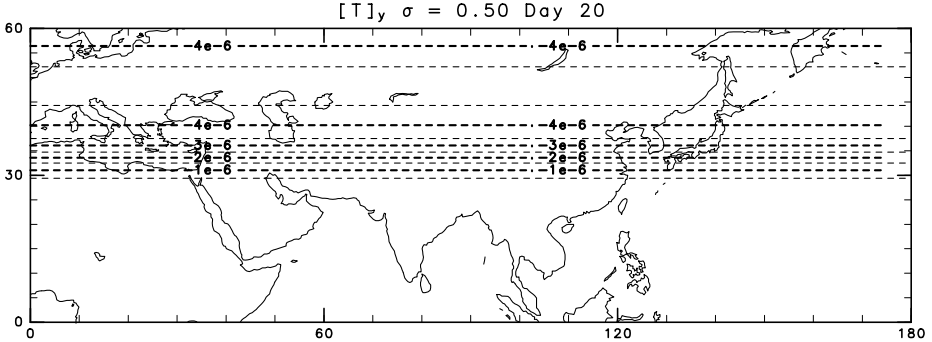

CONTOUR INTERVAL = 5.000E-07

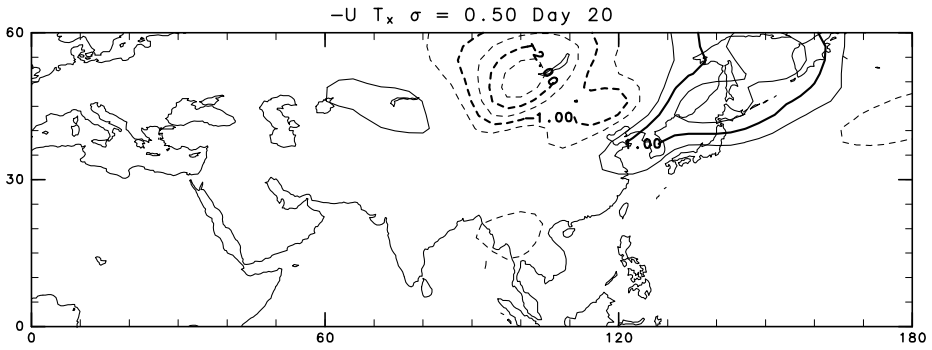

CONTOUR INTERVAL = 5.000E-01

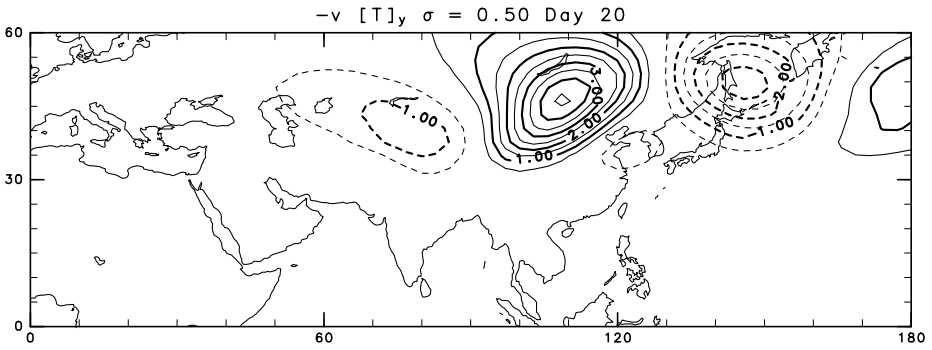

CONTOUR INTERVAL = 5.000E-01

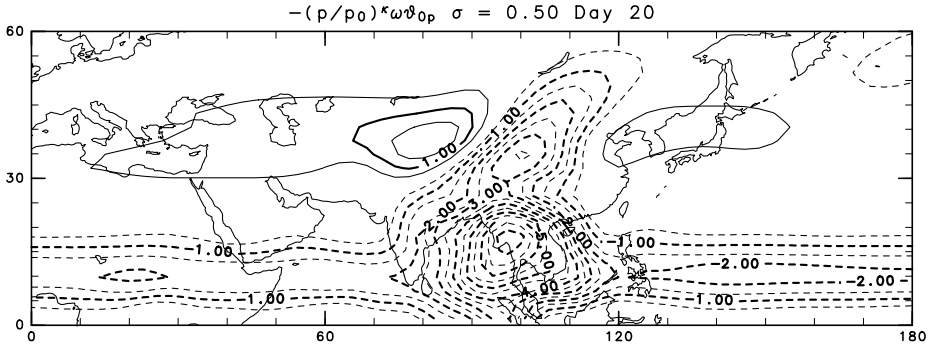

CONTOUR INTERVAL = 5.000E-01

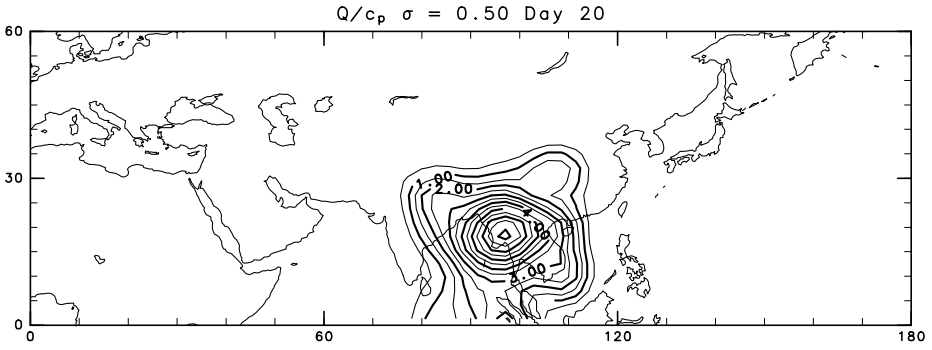

CONTOUR INTERVAL = 1.000E+00

Thermodynamic balance

$$\bar{u}\frac{\partial T'}{\partial x} + \frac{\partial \bar{T}}{\partial y}v' + \left(\frac{p}{p_0}\right)^{\kappa}\omega\frac{\partial \theta}{\partial p} = \frac{Q}{c_p}$$

At 40N on the 500 hPa surface

- $\bar{u} \sim 8\ \mathrm{m/s}, v' \sim 4\ \mathrm{m/s}$
- $|T'_x| \sim 0.05\ \mathrm{K/1000km} < |\bar{T}_y| \sim 0.4\ \mathrm{K/1000km}$
- Thus the primary balance exists between meridional and vertical advection at the centre of decent.

Role of the jet

The zonal (eastward) basic flow

- creates a meridional tilt of isentropes.
- advects negative voriticity eastward.

As a result, the meridional flow of disturbance has a vertical component, which induces the stationary Rossby wave.

Response to the Indian heating in the presence of the jet and orography

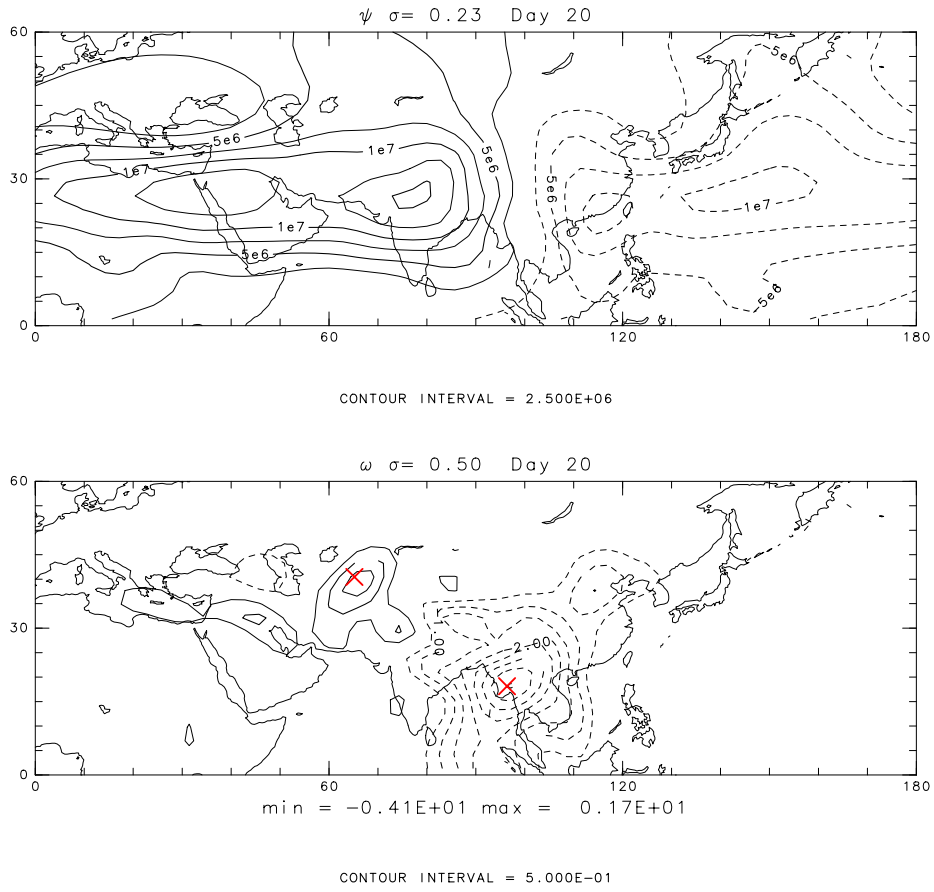

Figure 15: ψ at $\sigma = 0.23$ and ω at $\sigma = 0.5$

Response to the Indian heating in the presence of the jet and orography shifted $-45°$

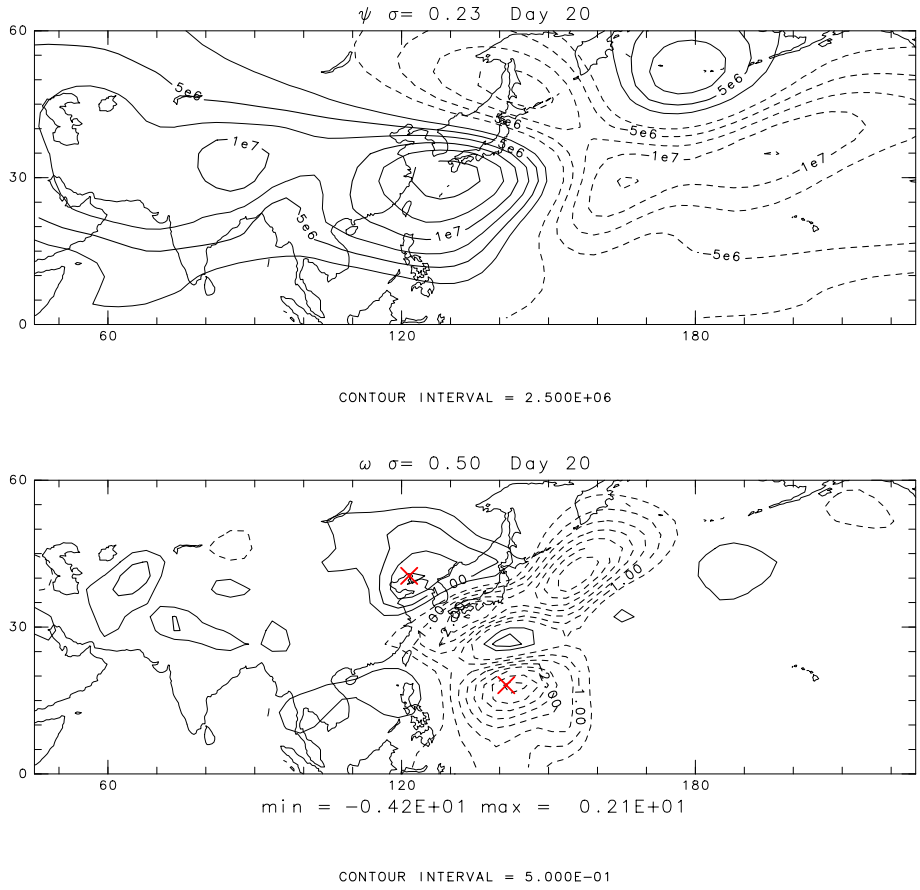

Figure 16: ψ at $\sigma = 0.23$ and ω at $\sigma = 0.5$

Stationary Rossby wave propagation

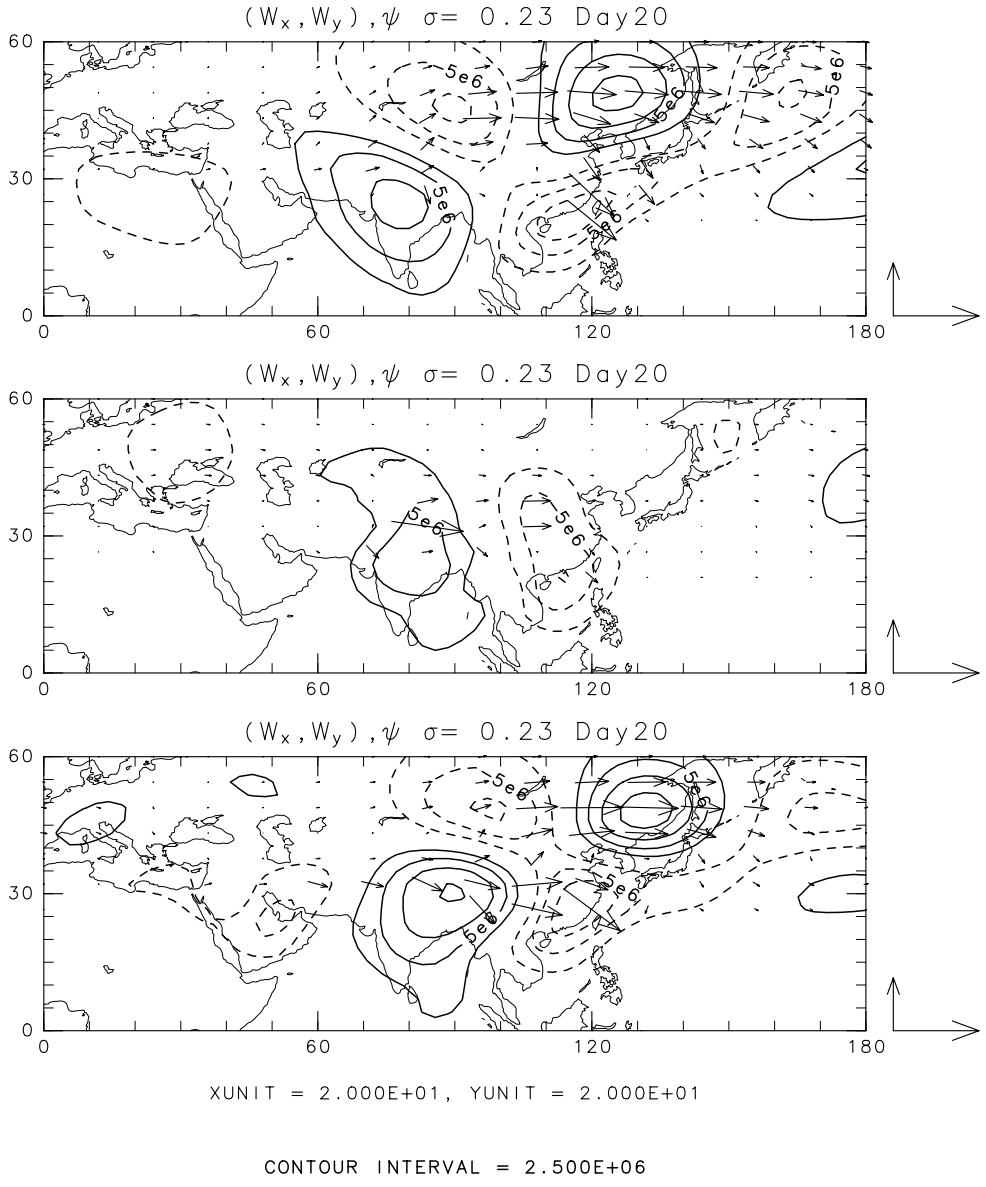

Figure 17: Wave activity flux on $\psi'(k \geq 3)$ for *without*, *with*, and *shifted* orography runs

Effect of orography

- The orography modifies distribution of vertical motion thus Rossby wave induction.
- Cancellation of the mechanical ascent and the thermally-induced explains why descent does not exist near the forcing and implies involvement of other processes.
- Weakening of vertical motion suppresses the Rossby wave induction.
- The descent near the Aral sea has a realistic location and distribution.

Which diabatic heating is important?

- Indian heating, jet, and orography: no Bonin high
- Other regions of diabatic heating/cooling:
  1. Western Pacific (110-180E, 5-25N)
     – PJ pattern (Nitta, 1987)
  2. Japan (120-150E, 30-60N)
  3. Silk Road (0-120E, 30-60N)

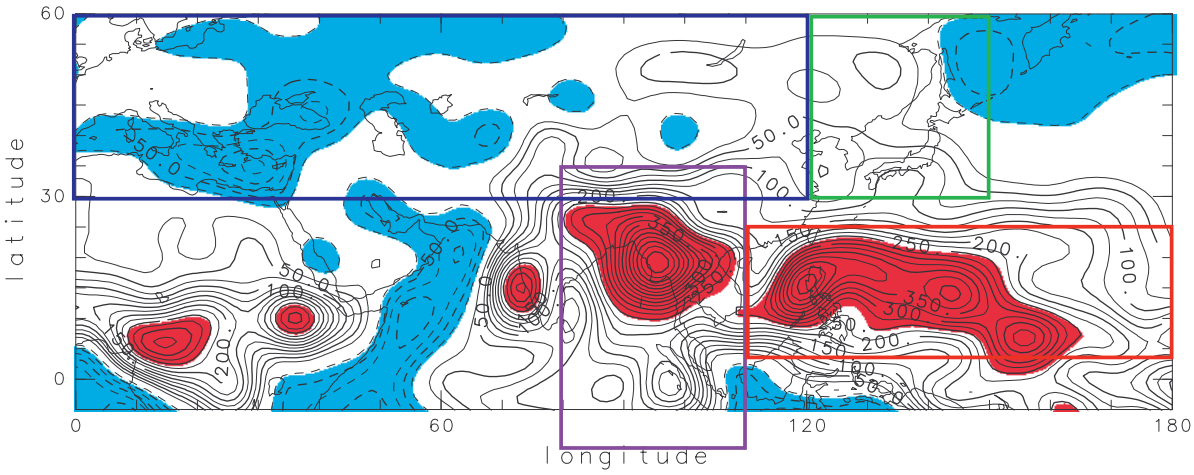

Fig 2: Column integrated diabatic heating in August (ERA15 climatology) in $\mathrm{W/m^2}$

Comparison: Upper troposphere

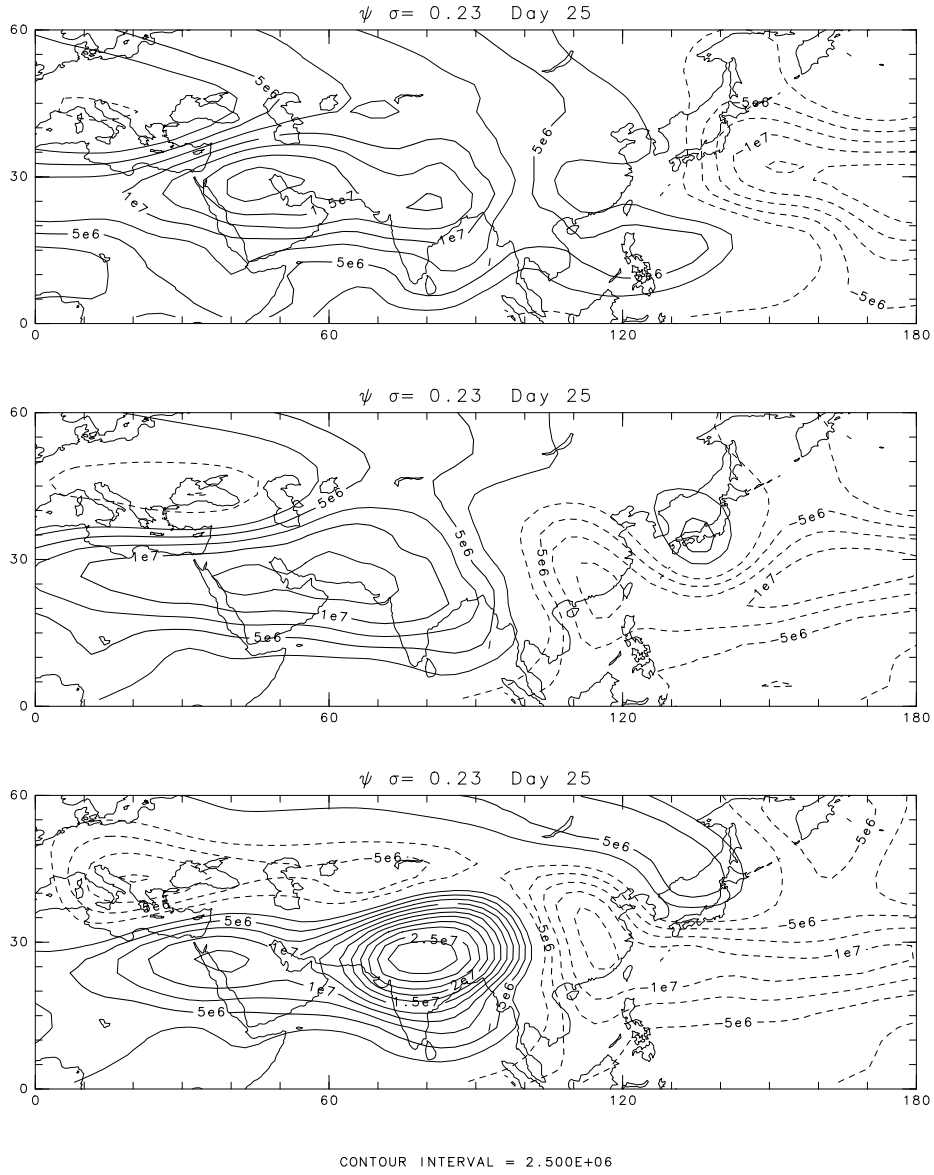

Figure 18: ψ at $\sigma = 0.23$ for *W Pacific*, *Japan*, and *Silk Road* runs.

Comparison: Surface pressure

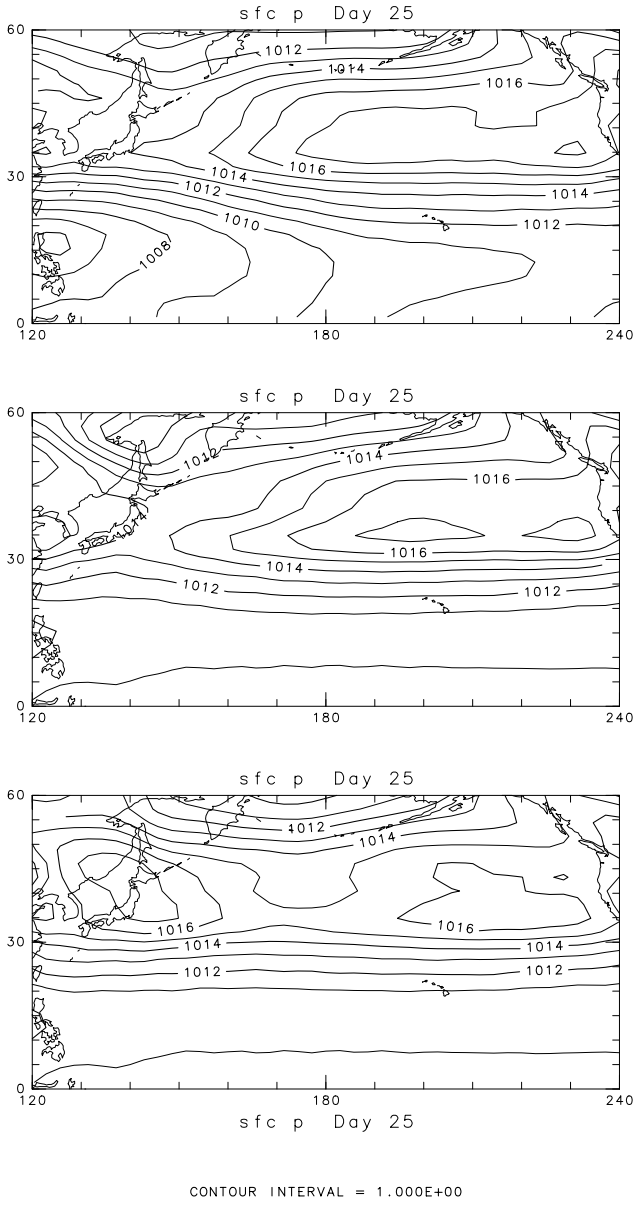

Figure 19: Sea level p for $W\ Pacific$, $Japan$, and $Silk\ Road$ runs.

Stationary Rossby wave from the desert

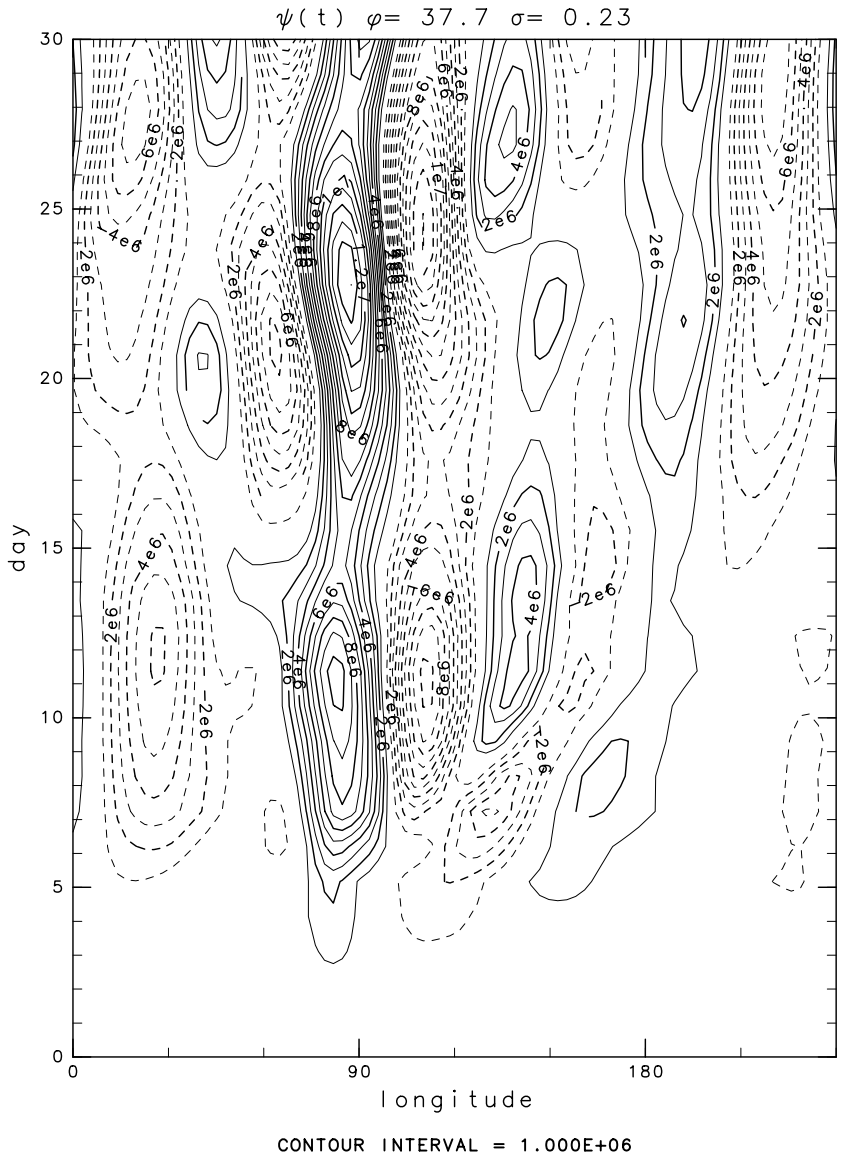

Figure 20: λ-t section of ψ'

Comparison: Wave activity flux and ψ'

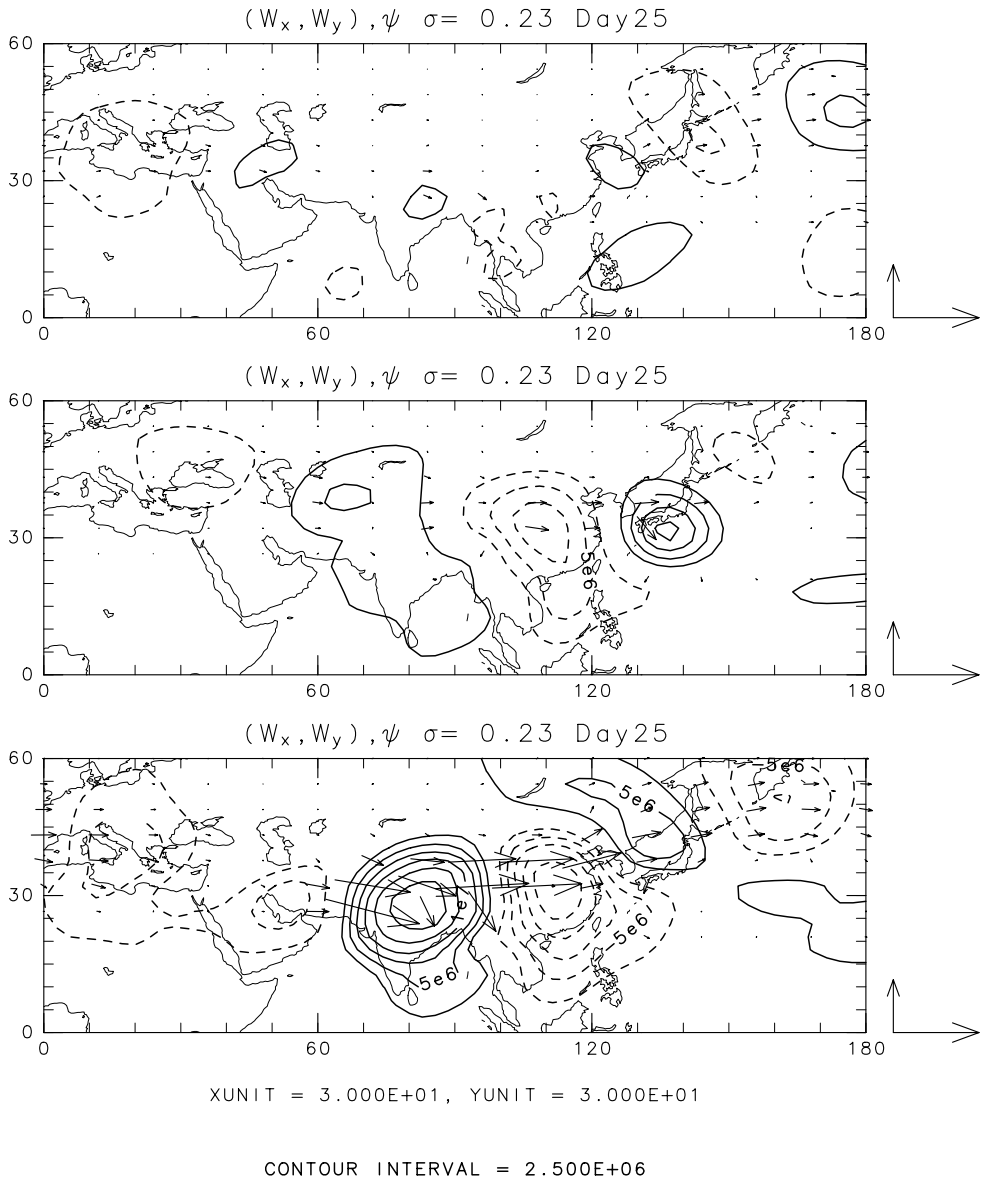

Figure 21: Wave activity flux on $\psi'(k \geq 3)$ at $\sigma = 0.23$ for *W Pacific*, *Japan* and *Silk Road* runs.

Nitta (1987)

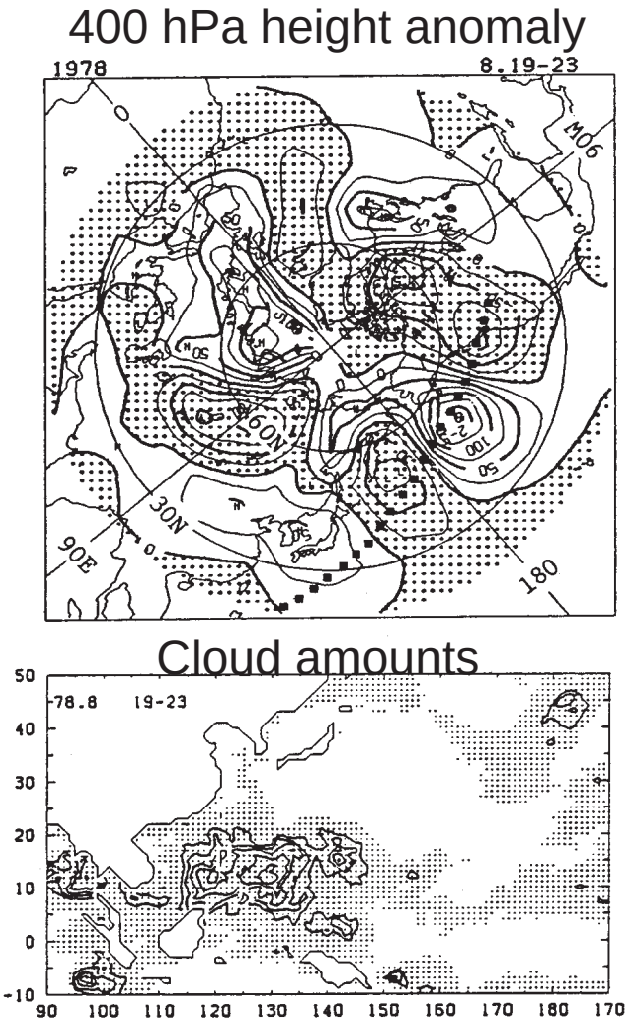

Fig. 14. Distributions of the height anomaly (m) at 400 mb (upper) and the cloud amount (lower) during 19–23 August, 1978. Negative height anomalies are shaded. Cloud amounts larger than 5.0 are contoured with the interval of 1.0 and areas with larger cloud amount than 1.0 are shaded. The dotted line denotes the great circle used for time sections.

Effect of other heating/cooling

- The Western Pacific heating appears to be important in the low levels and to induce the $PJ\ pattern$, which is not of primary importance to the equivalent-barotropic structure near Japan.

- The local diabatic forcing appears to enhance the upper tropospheric anticyclone over Japan. Its effect near the surface is minor.

- The Silk Road cooling is of primary importance in stationary Rossby wavepacket induction. The development of decay of anticyclone has timescale of ~ 10 days, which is consistent with observation.

Experiments with climatological heating

Having understood the role of various heating/cooling heat source, the jet, and orography, the climatological heating is used:

1. Total

2. Total but the Western Pacific heating

3. Total but the Silk Road (incl. Japan) cooling

Comparison: Upper troposphere

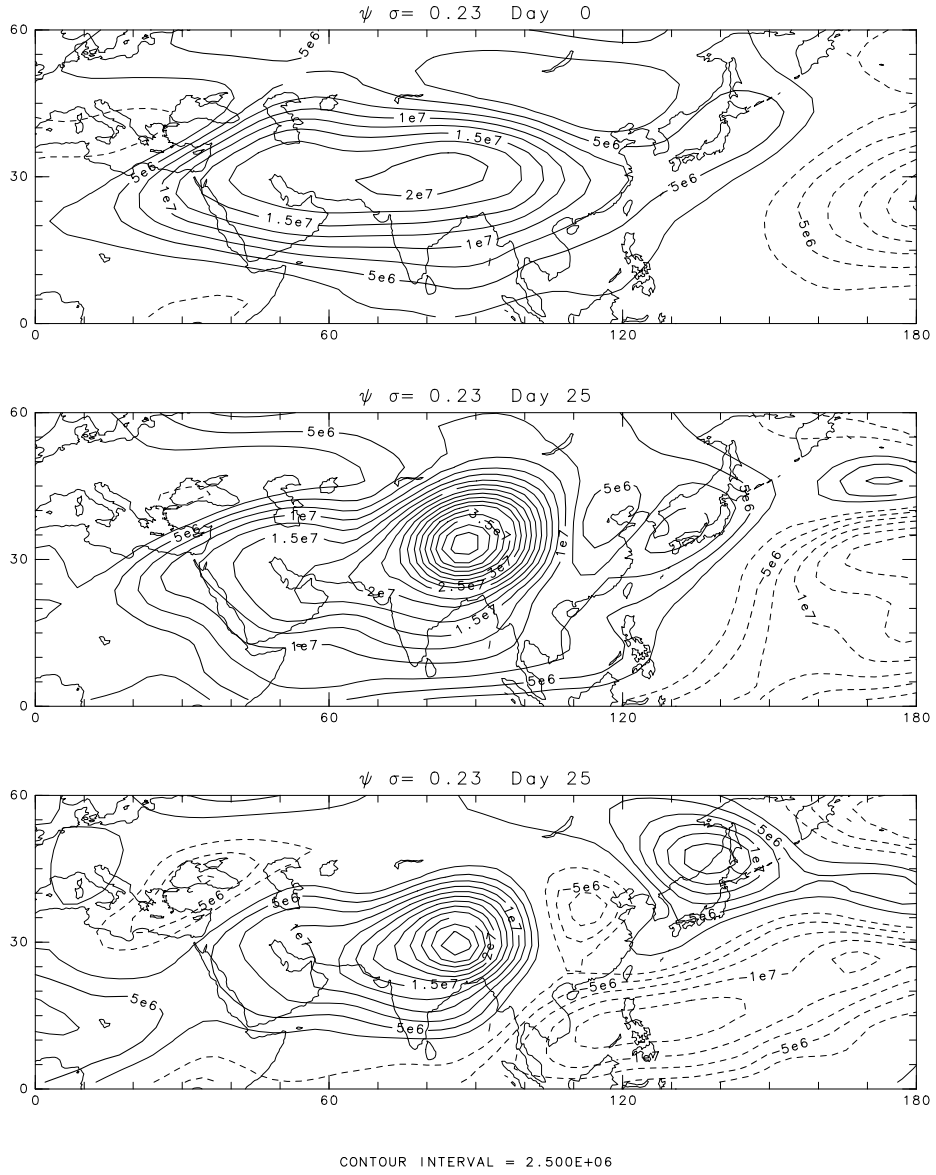

Figure 22: ψ at $\sigma = 0.23$ for the climatology, control and $no\ W\ Pacific$ runs.

Comparison: Upper troposphere

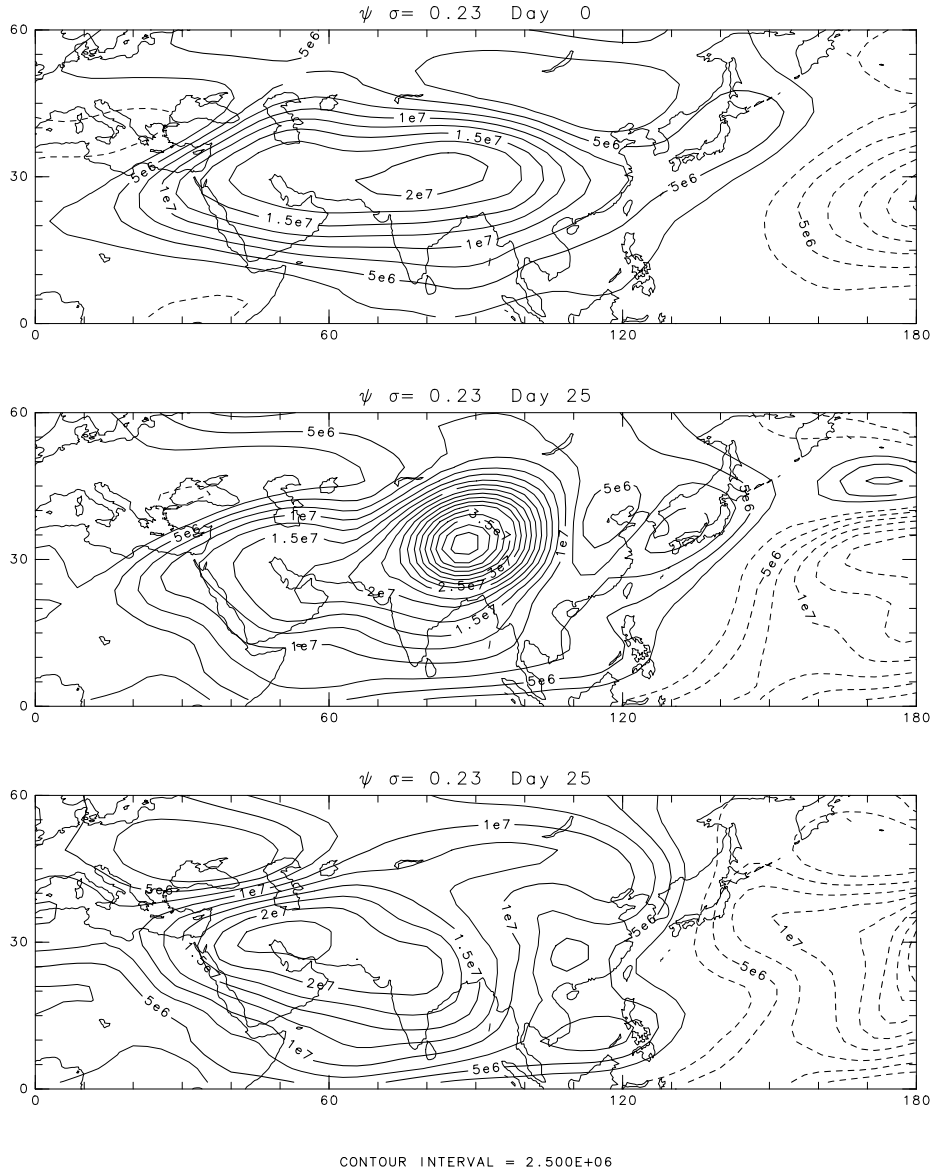

Figure 23: ψ at $\sigma = 0.23$ for the climatology, control and $no\ Silk\ Road$ runs.

Comparison: Surface pressure

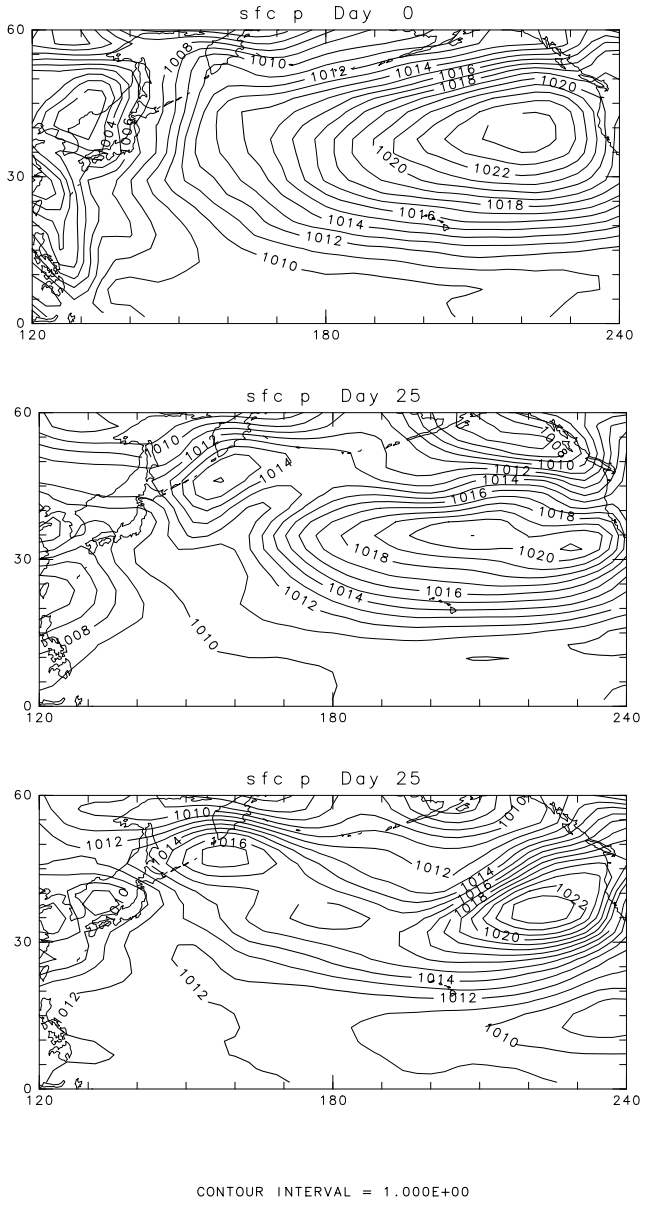

Figure 24: Sea level p for the climatology, control and $no\ W\ Pacific$ runs.

Comparison: Surface pressure

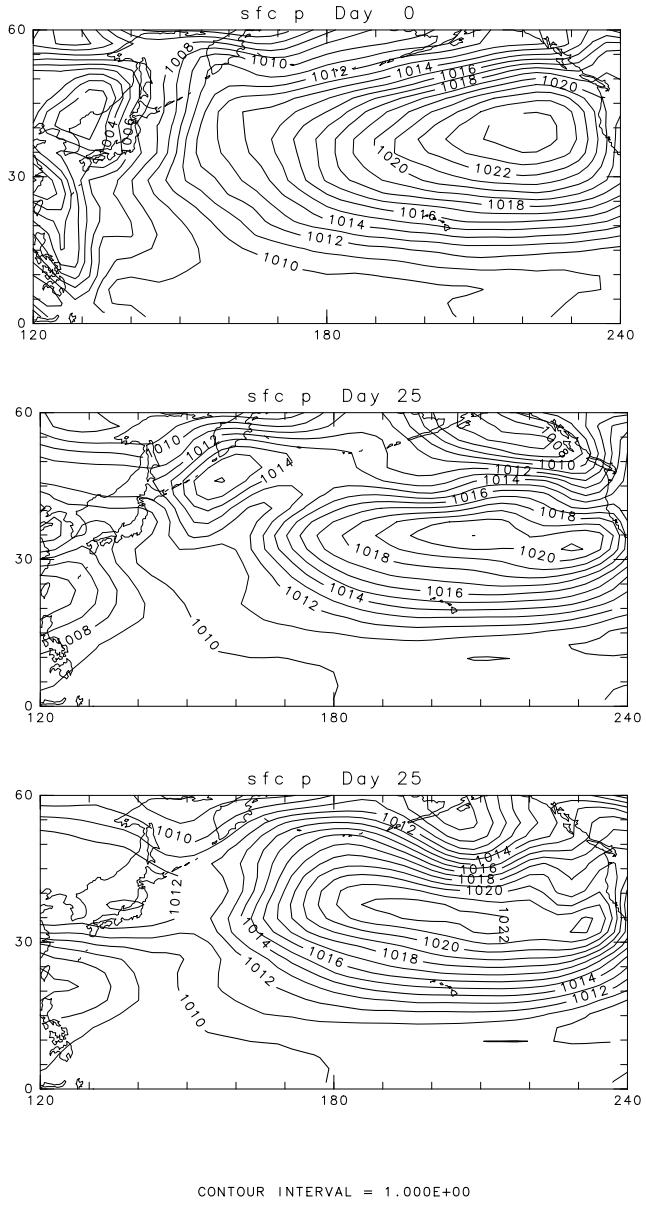

Figure 25: Sea level p for the climatology, control and *no Silk Road* runs.

Time evolution of ψ' in the Control

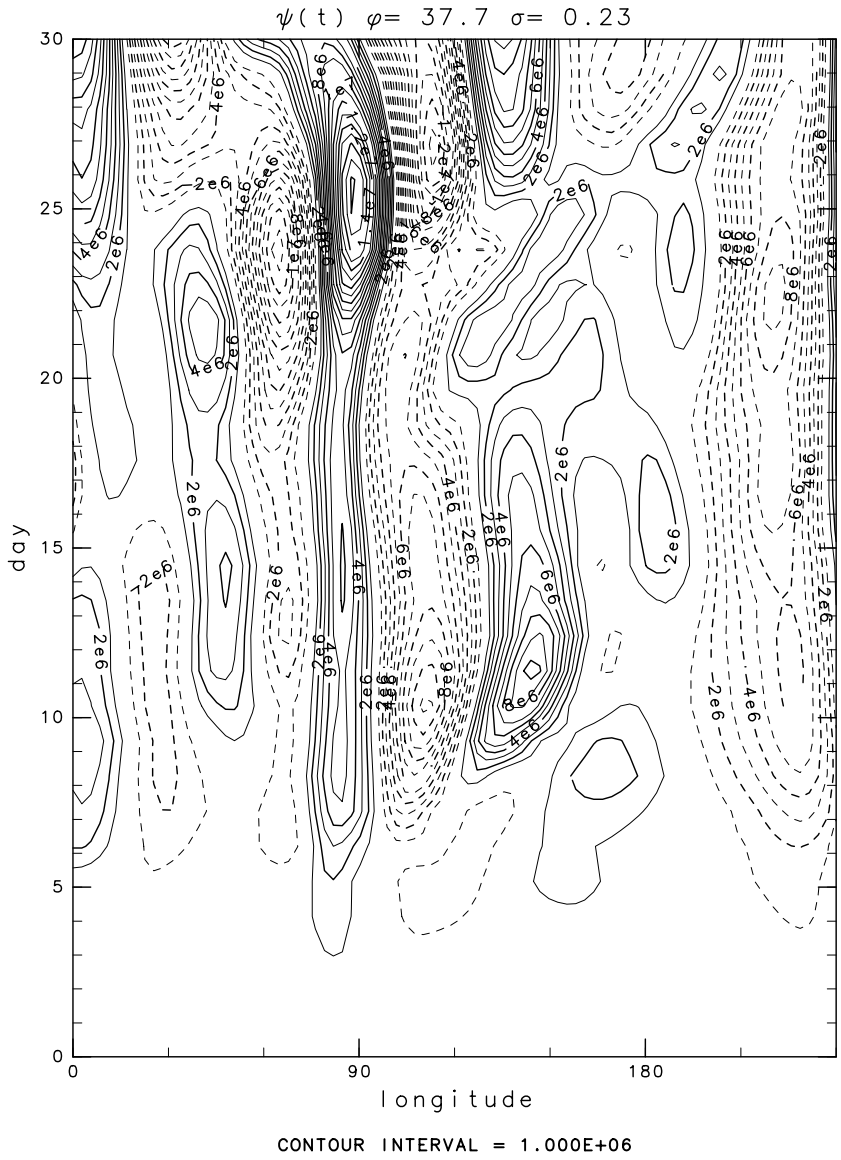

Figure 26: λ-t section of ψ' at $\phi = 38$N

Time evolution of ψ' in the *no W Pacific* run

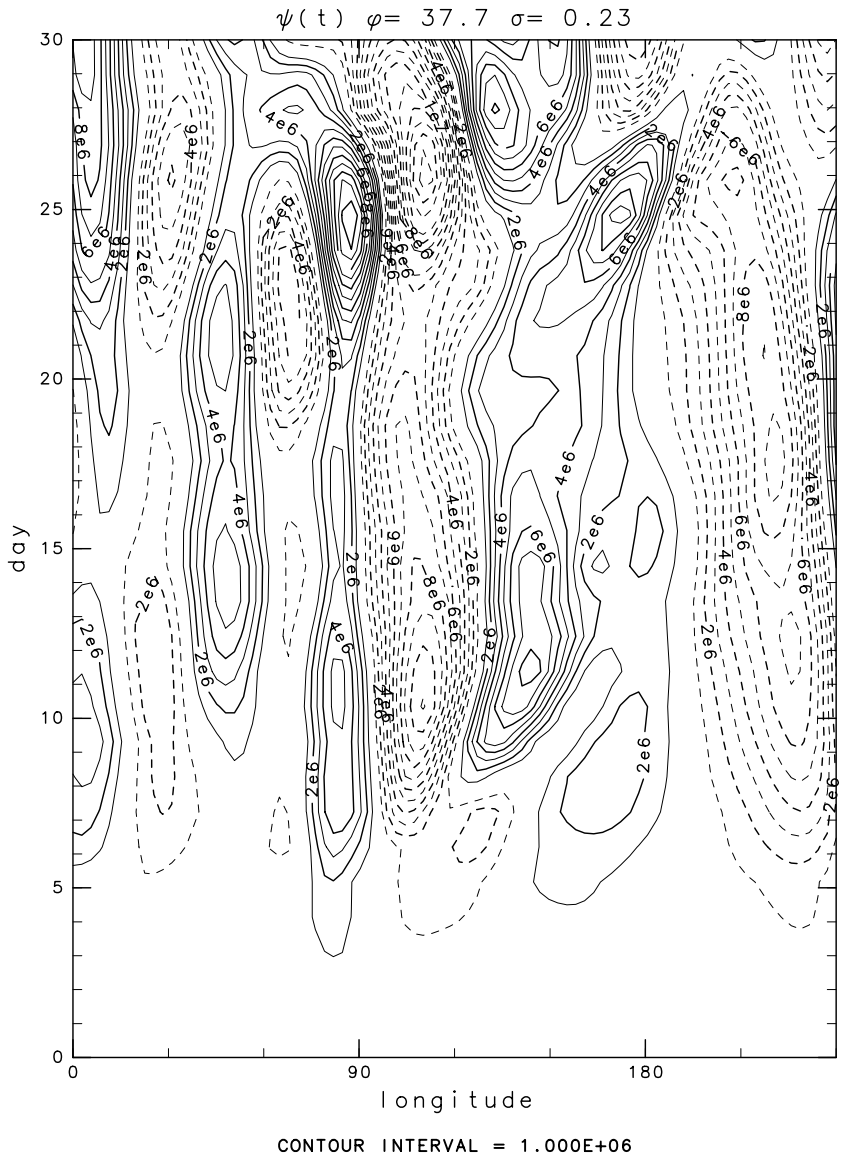

Figure 27: λ-t section of ψ' at $\phi = 38$N

Time evolution of ψ' in the *no Silk Road* run

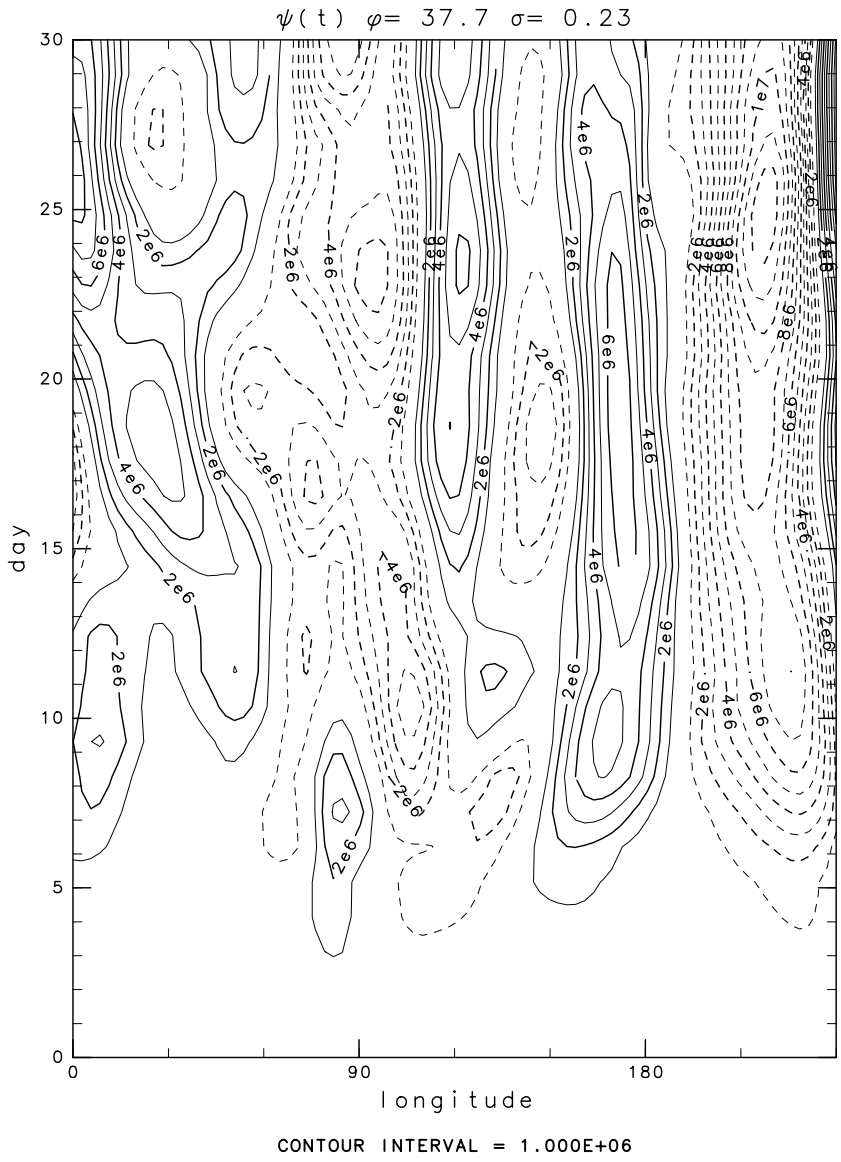

Figure 28: λ-t section of ψ'

Comparison: Wave activity flux and ψ' at $\phi = 38$N

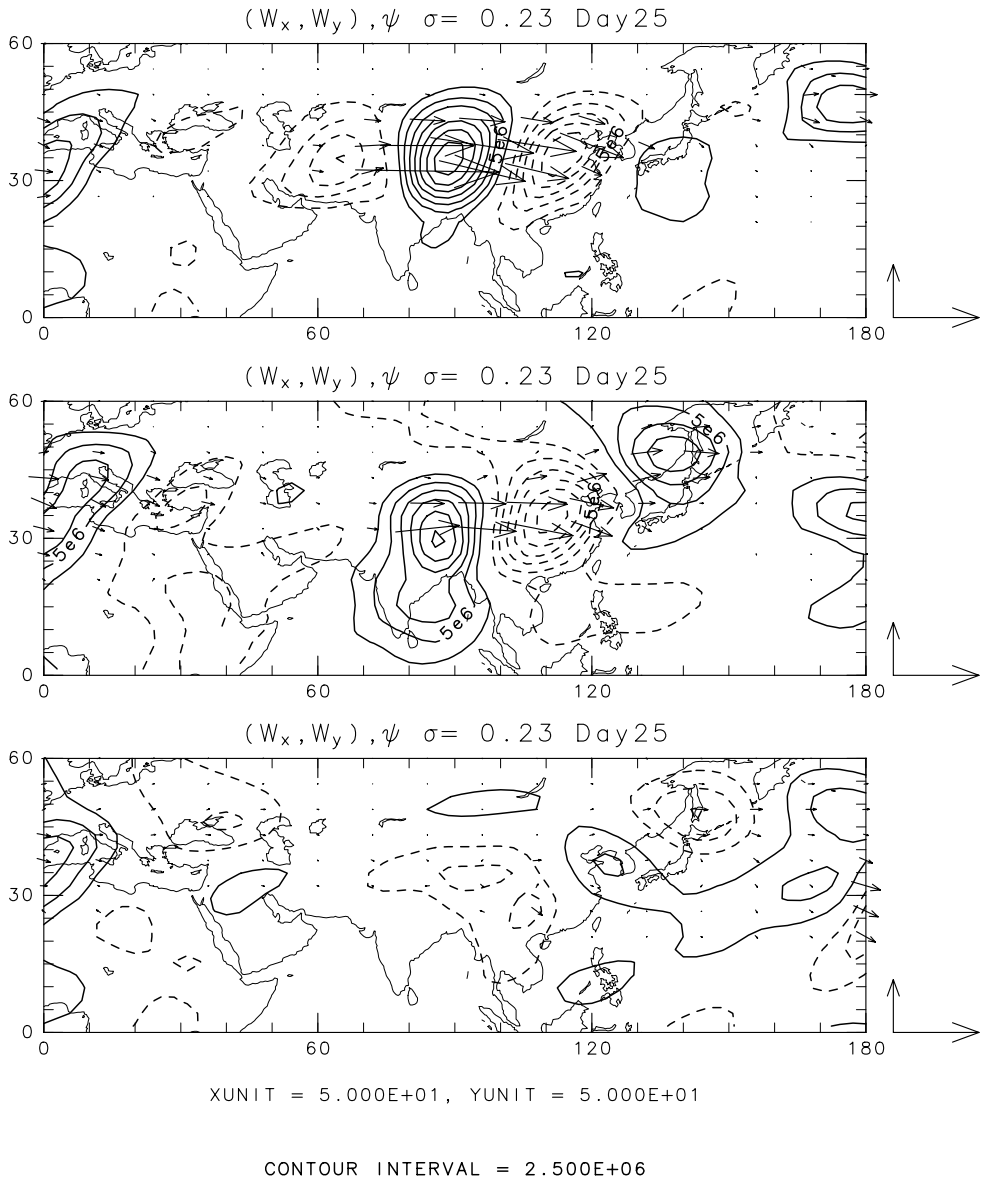

Figure 29: Wave activity flux on $\psi'(k \geq 3)$ at $\sigma = 0.23$ for the control, *no W Pacific* and *no Silk Road* runs

Comparison: Isentropic PV

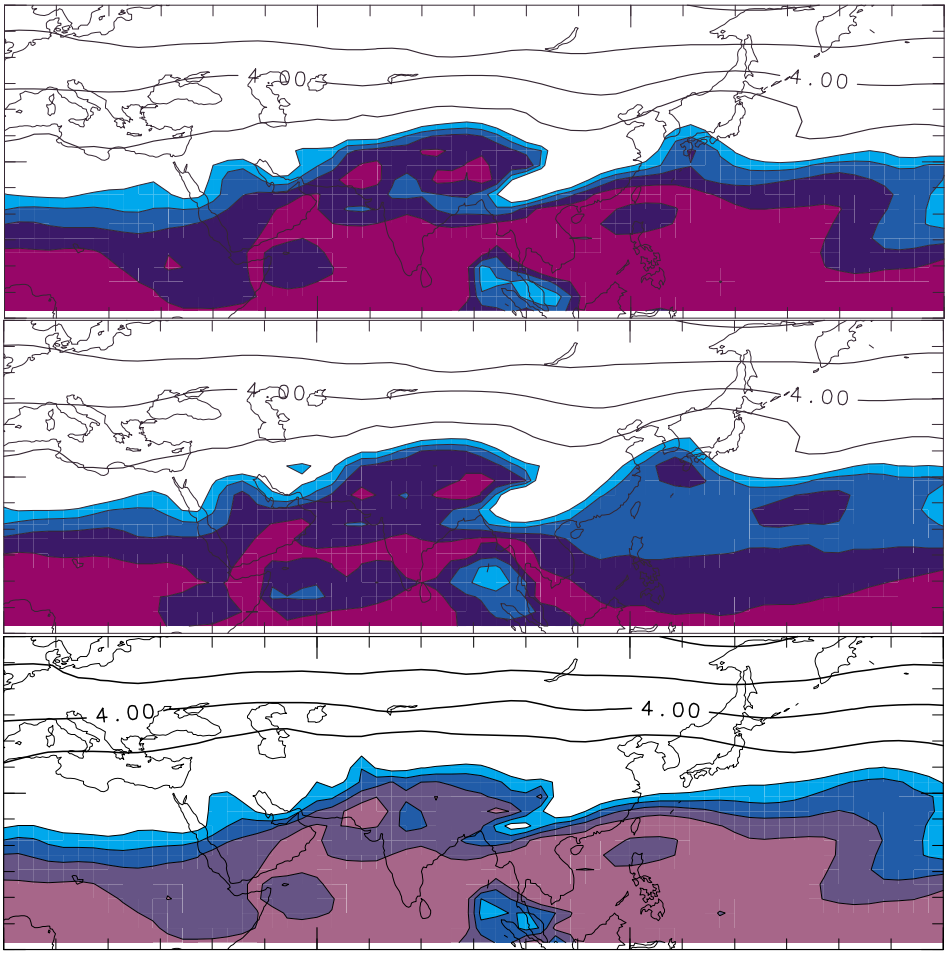

Figure 30: IPV on 350 K at Day 10 for the control, *no W Pacific*, and *no Silk Road* runs

Comparison: Isentropic PV

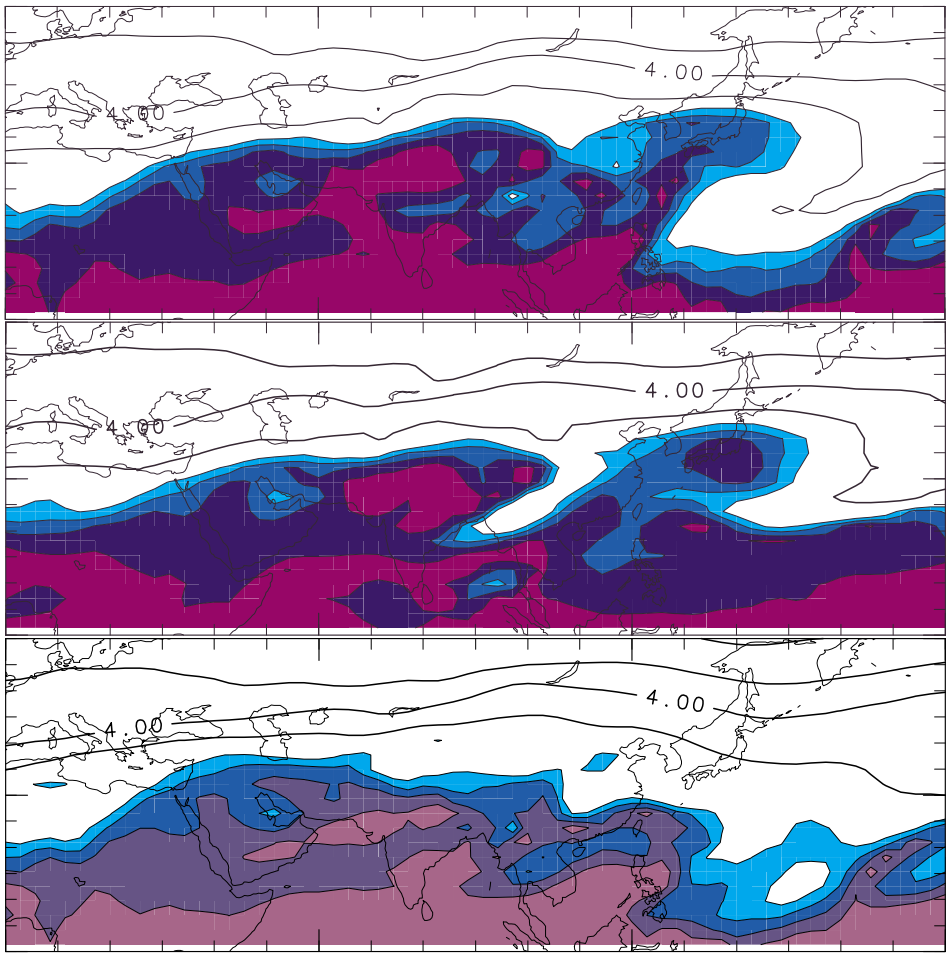

Figure 31: IPV on 350 K at Day 15 for the control, *no W Pacific*, and *no Silk Road* runs

Summary of climatological heating experiments

- The equivalent-barotropic anticyclone near Japan is successfully simulated with a simple GCM.
- The existence of anticyclone without the Western Pacific heating shows the lack of importance of this heating.
- Removal of the Silk Road cooling weakens the anticyclone: the remote descent creates the Bonin high.
- The develpment of anticyclone can be understood in terms of negative PV anomaly over Japan.

Mechanism for the Silk Road pattern and Bonin high

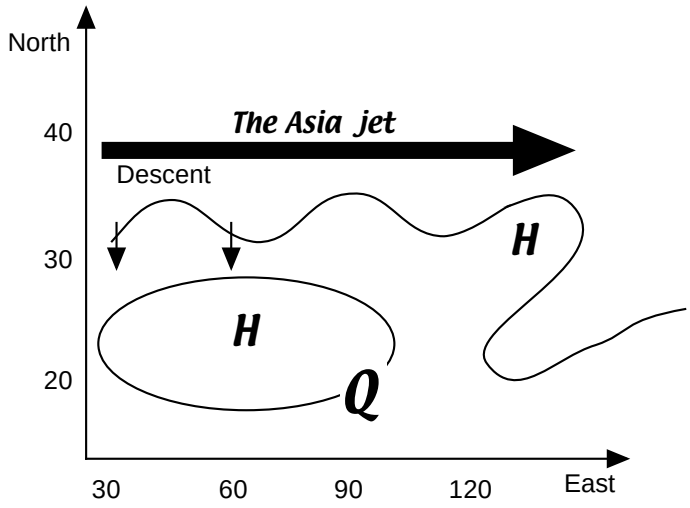

Figure 32: Schematic diagram illustrating mechanism for the Silk Road pattern and Bonin high

Conclusions

Base upon the foregoing dynamical consideration, climatology, and numerical experiments, the following hypothesis is proposed:

- The Indian heating, off the equator during the summer monsoon, creates the Asia jet and zonal temperature gradient.
- The descent near the Aral sea and East Mediterranean sea induces the stationary Rossby wave on the jet.
- The Rossby wavepacket propagates along the jet converges near Japan and creates the Bonin high.
- The Bonin high is enhanced by the local diabatic forcing. The PJ pattern may be in phase.

Corresponding author: ENOMOTO Takeshi eno@aos.eps.s.u-tokyo.ac.jp